June 21, 2007 **Version 1.1**

ABSTRACT

Name: Edward W. Nissen Department: Physics

Title: Chaos and its Role in Emittance Growth in Fixed Field Alternating Gradient Accelerators

Major: Physics Degree: Master of Science

Approved by: Date:

Thesis Director

NORTHERN ILLINOIS UNIVERSITY

ABSTRACT

This study involved modeling the actions of high space-charge beams in fixed field alternating gradient accelerators using a truncated model of the Fermilab booster. The study assumed a constant Gaussian particle distribution that was allowed to evolve along with the beam. The beam was modeled using a symplectic mapping algorithm, perturbed to account for space-charge. The analysis included a new tool for determining the chaos strength of an orbit as it evolves, which allowed for an analysis of when the beam has reached a resonance. Snapshots of the beam in trace-space, as well as the evolution of individual orbits showed that, in most of the space-charge regimes studied, emittance growth is carried out through particles becoming trapped in islands. These islands expand as the beam nears resonance and form the halo. Further analysis of the betatron-tune of the system showed that those cases where the island mechanism does not apply occur due to the space-charge preventing the betatron-tune from reaching resonance.

NORTHERN ILLINOIS UNIVERSITY

CHAOS AND ITS ROLE IN EMITTANCE GROWTH IN FIXED FIELD ALTERNATING GRADIENT ACCELERATORS

A THESIS SUBMITTED TO THE GRADUATE SCHOOL
IN PARTIAL FULFILLMENT OF THE REQUIREMENTS
FOR THE DEGREE
MASTER OF SCIENCE

DEPARTMENT OF PHYSICS

DEKALB, ILLINOIS
JUNE 2007

In accordance with departmental and Graduate School policies, this thesis is accepted in partual fulfillment of degree requirements

Certification:

_____

Thesis Director

_____

Date

DEDICATION

For my family

ACKNOWLEDGEMENT

A number of people and organizations have helped me perform this research whose contributions must be acknowledged. I would like to thank Professor Court Bohn who brought me into this group and this field. Though he is no longer with us his influence will carry on indefinitely. I would also like to thank Dr. Balša Terzić who stepped in and helped me finish both the research and this thesis. I would like to thank Dr. Ioannis Sideris for his early guidance, as well as his wonderful tool for evaluating chaos in a system. Finally I would like to thank the Directed Energy Professional Society for their generous Scholarship which helped me to focus my attention on completing my research.

TABLE OF CONTENTS

LIST OF TABLES

LIST OF FIGURES

CHAPTER 1
INTRODUCTION

As newer uses for charged particle beams become apparent, the abilities of fixed field alternating gradient accelerators becomes more desirable. Newer uses for charged particle beams often require more and more particles compressed into a smaller and smaller space, which increases the effect of space-charge and can lead to both chaotic motion and emittance growth to the point of halo formation.

Earlier studies with varying levels of self-consistency have focused on Gaussian shaped beam distributions in the transverse dimensions. These investigations showed a tendency for the emittance to increase as the betatron-tune reached resonance, thus forming a halo. Some models have focused on the presence of sextupole errors in a beam with a constant distribution function, studying how the change in the betatron tune or tuneshift effects the dynamics of the beam[1]. Other studies have shown that if the model is made more self-consistent then the space-charge and tuneshift alone can account for this emittance growth around resonance[2].

The research herein assumes a Gaussian-shaped distribution function that changes its standard deviation based on the distribution of the test particles after each turn. The parameters of the model assume a truncated version of the Fermilab booster ring. It will be seen that in this model the space-charge can lead to the formation of stable islands at the periphery of the beam, and that the changing

betatron tune causes these islands to move outwards, trapping particles in them and bringing them out to a halo.

CHAPTER 2
THEORETICAL TOOLS

2.1 Hamiltonian Under Consideration

In order to model a fixed field alternating gradient accelerator a suitable Hamiltonian must be chosen. Theoretically, it should be possible to model the initial conditions of every particle in the accelerator and determine how they interact with both the external magnetic fields used to focus the beam, and their interactions with each other. In the scope of this study values ranging from 1×10^9 to 1×10^{13} particles per meter are considered. Numbers in this range become computationally prohibitive. However, if we assume that the beam bunch maintains a given distribution function, then we can calculate the effect on a test particle by the rest of the beam using a smooth distribution.

The assumed distribution is:

$$\rho(x,z) \quad = \quad \frac{Ne}{2\pi\sigma_x\sigma_z} e^{-\frac{x^2}{2\sigma_x^2}-\frac{z^2}{2\sigma_z^2}}. \tag{2.1}$$

This is a Gaussian distribution in configuration space for the transverse axes x and z. This model only deals with the transverse dimensions, longitudinsl effects are not included. This distribution obeys the following Hamiltonian:

$$V(x,z) = \frac{Nr_0}{\beta^2\gamma^3}\int_0^\infty \frac{-1+e^{-\frac{x^2}{2\sigma_x^2+t}-\frac{z^2}{2\sigma_z^2+t}}}{\sqrt{(2\sigma_x^2+t)(2\sigma_z^2+t)}}dt, \tag{2.2}$$

where N is the number of particles per unit length, r_0 is the classical proton radius of value 1.5347×10^{-18}m. β and γ are the relativistic variables, σ_x and σ_z are the rms moments in the x and z directions and t is a dummy variable for integration.

2.2 What is Chaos?

The scope of this thesis considers the phenomenon of emittance growth in resonance crossings as they relate to the chaos of the system in question. Therefore, it is important to define chaos, as well as the manner in which we measure it.

During the course of this work, frequent mention will be made to either chaotic or regular orbits. A regular orbit is defined as a well-behaved, closed orbit whose coordinates in phase-space (in this study trace-space) follow smooth curves. A regular orbit can be predicted out to infinity. An example of the signal of a regular orbit is found in Figure 2.1.

On the other hand, a chaotic orbit is an orbit whose end result depends sensitively on its initial condition. In such a chaotic regime, the closely spaced initial conditions will diverge exponentially in time. Therefore, accurately predicting the location of a particle after it has been advanced through time becomes impossible after a certain point, which is dependent on how chaotic the particle's trajectory is. An example of a chaotic orbit's signal is found in Figure 2.3

It should be noted that there is a distinction between chaotic motion and random motion. Chaotic motion is fully deterministic – it merely depends on initial

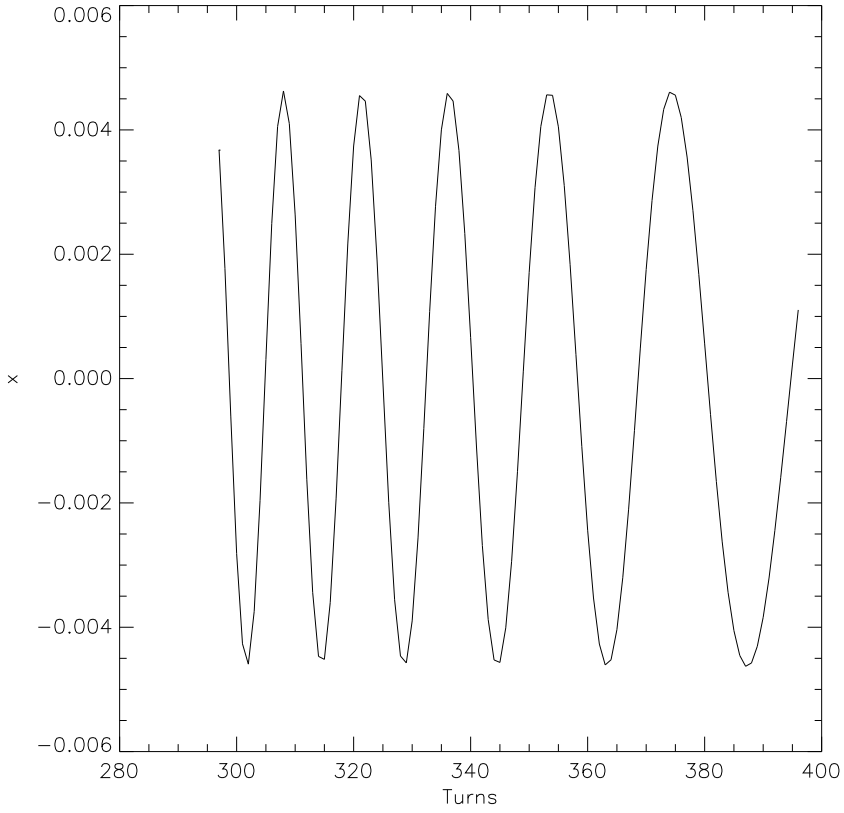

Figure 2.1: An example of the signal of a regular orbit.

conditions to the point that we can only make predictions out to a certain time with any confidence.

The most common method of determining how chaotic an orbit is involves calculating the largest Lyapunov exponent. This is defined as the natural logarithm of the average divergence between initially closely-spaced particles:

$$\lambda = \lim_{t\to\infty} \lim_{|\Delta x_0|\to 0} \frac{1}{t} \ln \frac{|\Delta x(t)|}{|\Delta x(0)|} \tag{2.3}$$

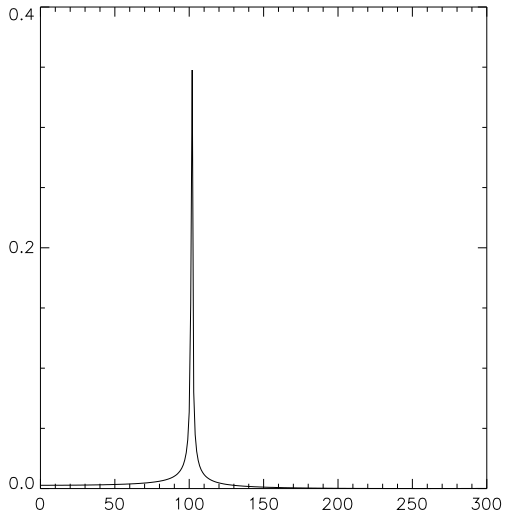

Figure 2.2: An example of a regular power spectrum. (Arbitrary units.)

Other measures involve determining the spectrum of frequencies contained in an orbit. As we can see in Figure 2.2, a regular orbit features only a few discrete frequencies, while a chaotic orbit has a broad spectrum as is seen in Figure 2.4.

There is a third category that will be used herein, and that is sticky orbits. A sticky orbit is an orbit that exhibits chaotic motion, but during certain epochs appears regular, and can exhibit semi-regular behavior. An example of the signal of a sticky orbit can be seen in Figure 2.5.

2.3 Patterns Method

One difficulty with most measures of chaos is that they only measure the overall chaoticity of an orbit, and do not give information about how regular or chaotic an orbit is at a given time. Fortunately, former Northern Illinois University

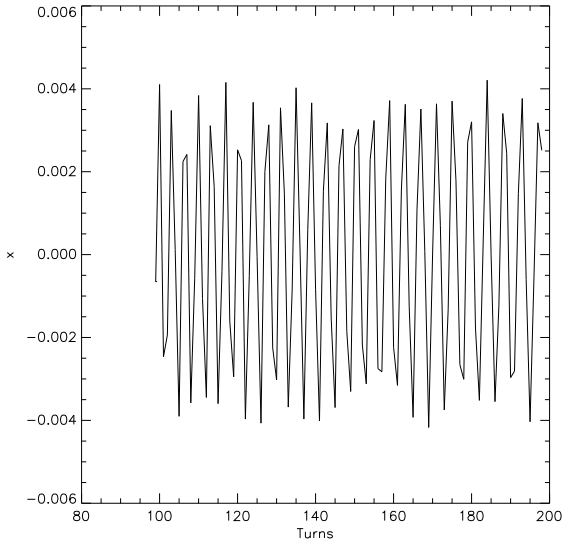

Figure 2.3: An example of the signal of a chaotic orbit.

Beam Physics and Astrophysics member Dr. Ioannis Sideris developed a measure that can quantify the chaos of an orbit in a point-by-point manner. It is called the "patterns method"[3].

As was stated previously, in a regular orbit it is possible to draw all points as part of a smooth curve. Such a smooth curve is a useful way to characterize how regular an orbit is. The patterns method works by searching for these smooth curves within an orbit, and determining how accurately each point fits within these curves. These smooth curves may be interweaved with each other: for instance in Figure 2.6 there are five curves.

In order to determine how closely a point adheres to a smooth curve, the method looks at the other points on the smooth curve, and interpolates what the

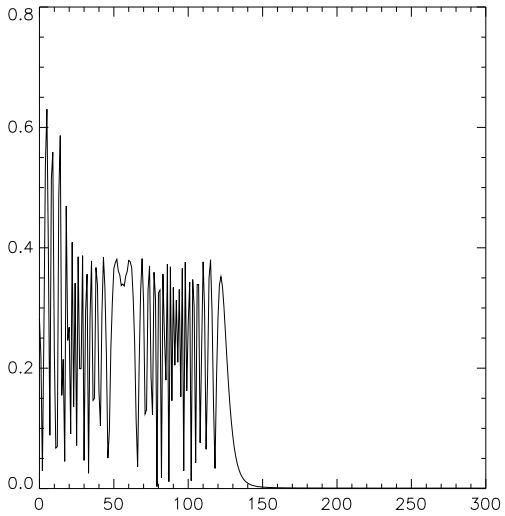

Figure 2.4: An example of a chaotic power spectrum. (Arbitrary units.)

curve expects the value to be at that point. In Figure 2.6, if we were interested in point 4 we would compare it to the value interpolated between points 0 and 9, then determine the relative interpolation error which is defined as $\sigma = |(x_{real} - x_{interpolated})/x_{real}|$. Since we do not know a priori what the number of smooth curves will be, the method searches all possible numbers of curves and keeps the smallest relative interpolation error for each point (which corresponds to the curve it most closely resembles).

This ability to track the chaoticity of orbits as they evolve allows us to see features such as stickiness that were not visible before. Therefore, we can now see under what conditions an orbit becomes chaotic, what brings this about, and what the final effect is.

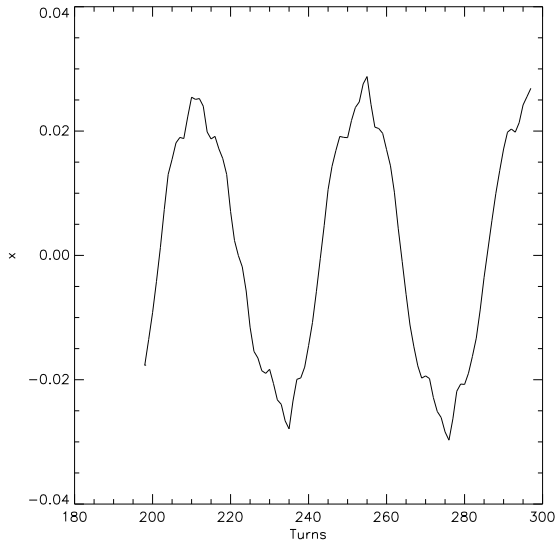

Figure 2.5: An example of the signal of a sticky orbit.

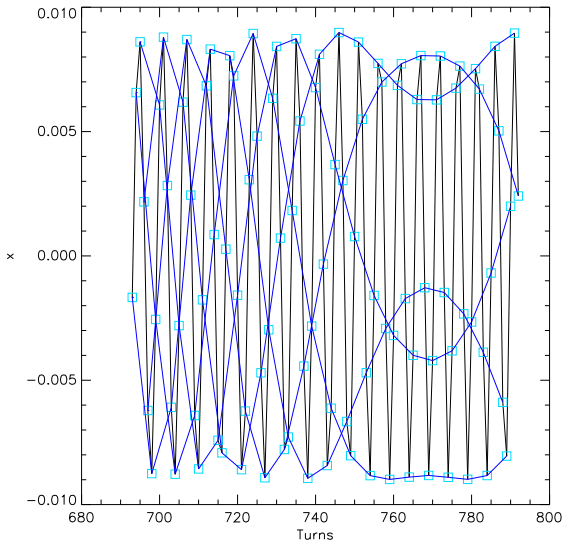

Figure 2.6: An example of underlying smooth curves in an orbit.

CHAPTER 3
NUMERICAL METHODS

3.1 The Integrator

Since the orbits are to be integrated through a large number of turns (1000 in the experiments shown) direct numerical integration (i.e. Runge-Kutta type) is inappropriate. Therefore, we model the beam using a perturbed symplectic (i.e. energy conserving) mapping algorithm.

What we model here is an accelerator ring with 24 focusing-defocusing cells (FODO) which cause the particles' coordinates to rotate in trace-space. The basic map is split into two half-cell transfer matrices which advance a beam through trace-space according to their respective focusing strengths[2].

First we map the coordinates going from the focusing to the defocusing section:

$$M_{F\to D} = \begin{pmatrix} \sqrt{\frac{\beta_{xD}}{\beta_{xF}}}\cos(\psi_x) & \sqrt{\beta_{xD}\beta_{xF}}\sin(\psi_x) & 0 & 0 \\ -\frac{1}{\sqrt{\beta_{xD}\beta_{xF}}}\sin(\psi_x) & \sqrt{\frac{\beta_{xF}}{\beta_{xD}}}\cos(\psi_x) & 0 & 0 \\ 0 & 0 & \sqrt{\frac{\beta_{zD}}{\beta_{zF}}}\cos(\psi_z) & \sqrt{\beta_{zD}\beta_{zF}}\sin(\psi_z) \\ 0 & 0 & -\frac{1}{\sqrt{\beta_{zD}\beta_{zF}}}\sin(\psi_z) & \sqrt{\frac{\beta_{zF}}{\beta_{zD}}}\cos(\psi_z) \end{pmatrix}, \tag{3.1}$$

Then we map from the defocusing to the focusing sections:

$$M_{D\to F} = \begin{pmatrix} \sqrt{\frac{\beta_{xF}}{\beta_{xD}}}\cos(\psi_x) & \sqrt{\beta_{xD}\beta_{xF}}\sin(\psi_x) & 0 & 0 \\ -\frac{1}{\sqrt{\beta_{xD}\beta_{xF}}}\sin(\psi_x) & \sqrt{\frac{\beta_{xD}}{\beta_{xF}}}\cos(\psi_x) & 0 & 0 \\ 0 & 0 & \sqrt{\frac{\beta_{zF}}{\beta_{zD}}}\cos(\psi_z) & \sqrt{\beta_{zD}\beta_{zF}}\sin(\psi_z) \\ 0 & 0 & -\frac{1}{\sqrt{\beta_{zD}\beta_{zF}}}\sin(\psi_z) & \sqrt{\frac{\beta_{zD}}{\beta_{zF}}}\cos(\psi_z) \end{pmatrix}, \tag{3.2}$$

Where β_{xF}, β_{xD}, β_{zF}, and β_{zD} are the focusing strengths, and ψ_x and ψ_z are the phase advances per half-cell given as $\frac{2\pi}{N_{halfcells}}\nu_{x,z}$ where $N_{halfcells}$ is the number of half-cells and $\nu_{x,z}$ are the betatron tunes for the respective dimensions. After each FODO cell we simulate an acceleration by linearly increasing the relativistic value of γ. The betatron-tune, or "tune", is the number of complete revolutions the particle makes in trace-space per turn through the accelerator.

3.2 Space Charge

Since there are multiple particles traveling through the accelerator we must find a way to describe the fields of the various particles of the beam on each test particle. Since we are using a symplectic mapping algorithm, we introduce forces as kicks of integrated strength to the x' and z' coordinates.

In order to use space-charge we must determine an expression for the force on a test particle. This is done by expanding the Hamiltonian found in Chapter 2 into a Taylor series:

$$
\begin{aligned}
V(x,z) &= \frac{Nr_0}{\beta^2\gamma^3}\int_0^\infty \frac{-1+e^{-\frac{x^2}{2\sigma_x^2+t}-\frac{z^2}{2\sigma_z^2+t}}}{\sqrt{(2\sigma_x^2+t)(2\sigma_z^2+t)}}dt \qquad (3.3)\\
&= \frac{Nr_0}{\beta^2\gamma^3}\left(\frac{x^2}{\sigma_x(\sigma_x+\sigma_z)}+\frac{z^2}{\sigma_z(\sigma_x+\sigma_z)}\right)\\
&- \frac{Nr_0}{4\beta^2\gamma^3\sigma_x^2(\sigma_x+\sigma_z)^2}\left(\frac{2+R}{3}x^4+\frac{2}{R}x^2z^2+\frac{1+2R}{3R^3}z^4\right),
\end{aligned}
$$

which, when we take the gradient to find the force and integrate over the half-cell length l, yields the trace-space kicks:

$$\Delta x' = -\frac{\partial V}{\partial x}l \approx \frac{2Nr_0 l}{\beta^2\gamma^3\sigma_x(\sigma_x+\sigma_z)}xe^{-\frac{x^2+z^2}{(\sigma_x+\sigma_z)^2}}, \qquad (3.4)$$

$$\Delta z' = -\frac{\partial V}{\partial z}l \approx \frac{2Nr_0 l}{\beta^2\gamma^3\sigma_z(\sigma_x+\sigma_z)}ze^{-\frac{x^2+z^2}{(\sigma_x+\sigma_z)^2}}. \qquad (3.5)$$

These kicks are applied to the x' and z' coordinates before each half-cell. Since we are interested in the resonance crossing, we linearly ramp the tunes from their starting values. σ_x and σ_z are calculated by finding the rms moments of all of the test particles after each turn. This was accomplished by splitting the integrator into two separate programs. The first integrates each particle one turn at a time and makes a snapshot of the beam at that given time. The second takes the statistical properties calculated for each turn, and uses them to integrate individual particle orbits. The algorithm is detailed in Figure 3.1.

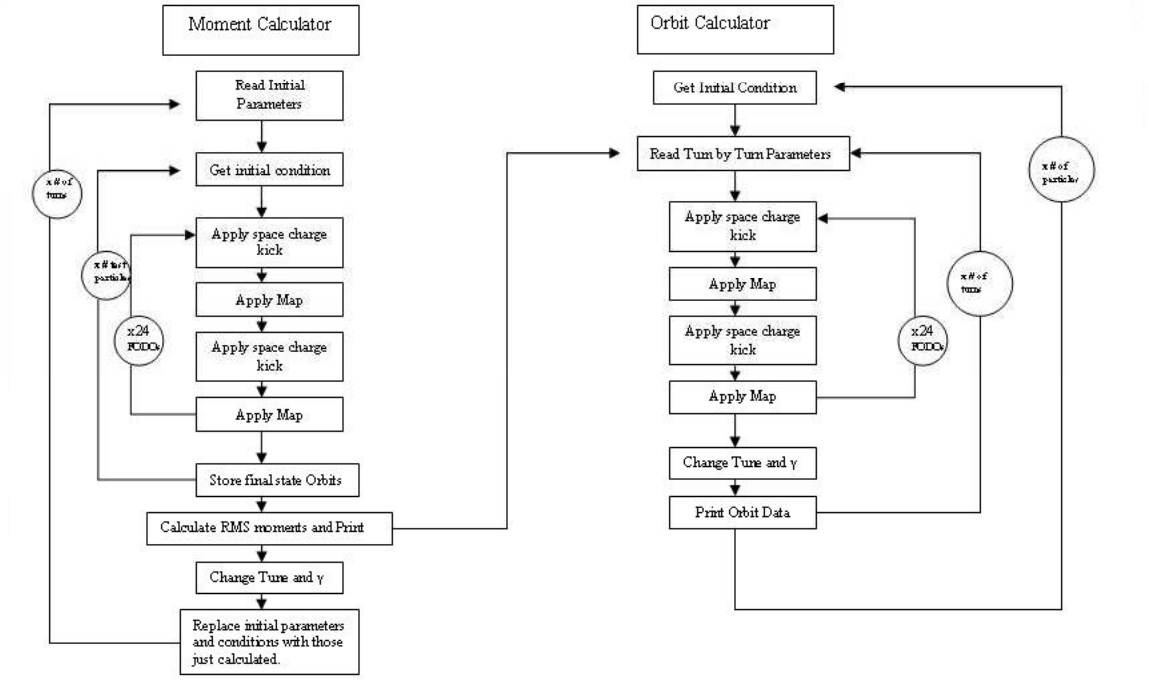

Figure 3.1: The software used.

3.3 Parameters Used

To aid in the efficient variation of parameters, important values are read from a separate file. An example would be:

1 MST413f

1.0e13 24 3.6 .018439 .0083 .7131 .9230 4.25 4.20 40.0 8.3 6.3 21.4 -.5 15000

For relevant values see Table 3.1.

The initial conditions follow a Gaussian distribution in configuration space. We are modeling a cold beam so the initial x' and z' values are zero. Since these are

Table 3.1: The parameters input into the integrator.

Symbol	Value	Description
npar	(varies)	number of parameters saved to the given file
outfile	(varies)	the file the rms moments or orbit trajectories saved to
N	(0.0-1×10^{13})	number of particles per meter
n_{cell}	24	number of complete FODO cells
$2l$	3.6	the length of the full FODO cell
σ_{x0}	0.0184	initial rms value of x
σ_{z0}	0.0083	initial rms value of z
β_0	0.7131	initial longitudinal velocity in units of c
β_f	0.9230	final longitudinal velocity in units of c
ν_{x0}	4.25 or 6.25	initial x betatron tune
ν_{z0}	4.20 or 6.20	initial z betatron tune
β_{xF}	40.0 m	x focusing strength
β_{zF}	8.3 m	z focusing strength
β_{xD}	6.3 m	x defocusing strength
β_{zD}	21.4 m	z defocusing strength
dir	-0.5	tune ramp rate translates to 0.00055/turn downramp
Ntest	5000-15000	number of test particles (only used to find moments)

randomly generated positions, we do not allow any that lie outside an ellipse with semi-major axis of 0.04 m and semi-minor axis 0.02 m (x and z respectively). To cover a wide range of possible space charge effects, we tested the values 0, 1×10^9,

5×10^9, 2.5×10^{10}, 5×10^{10}, 2.5×10^{11}, 5×10^{11}, 2.5×10^{12}, 5×10^{12}, and 1×10^{13} particles per meter.

3.4 Analytical Methods

There are several quantities of statistical and physical importance that were derived in this study. Some are calculated while the orbits are integrated, and others are retrieved from the data.

3.4.1 Statistical Properties

First, we must find the various rms moments since they are required for the integration. These are the rms values for position and trace space momentum:

$$\sigma_x = \sqrt{\frac{\sum_{i=1}^{N}(x_i - \overline{x})^2}{N}}. \tag{3.6}$$

A similar operation is used to find the $\sigma_{x'}$. The cross moments must also be determined, and are found using:

$$\sigma_{xx'} = \sqrt{\frac{\sum_{i=1}^{N}(x_i - \overline{x})(x_i' - \overline{x'})}{N}}. \tag{3.7}$$

We can then use these moments to determine the emittance. This is the area of trace space that the beam occupies. It is calculated from the rms moments of a beam:

$$\epsilon_x = \sqrt{\sigma_x^2 \sigma_{x'}^2 - \sigma_{xx'}^2}. \tag{3.8}$$

3.4.2 Trace Space Cross Sections

In order to view how the beam reacts to its various perturbations, we look at cross-sections of the beam at various times. This can be used to show how the beam as a whole reacts to the forces acting on it. When the analysis is performed, we will see the formation, progression and dissolution of the islands in the beam as resonance conditions are reached.

3.4.3 Tune Mapping

While theoretically we control the tune through ramping, the space-charge force can change the way the beam moves in such a way that a different fraction of the overall betatron wavelengths are completed in a turn. To determine the new tune with space-charge included, we assume that the beam has passed through a turn with no space-charge and see what tune would have produced the observed transformation:

$$x_1 \quad = \quad x_0 \cos(2\pi\nu_x) + \beta_{xF} x_0' \sin(2\pi\nu_x). \tag{3.9}$$

There will be some instances in which the space-charge force is so strong that there is no tune that can account for this behavior. Furthermore, there will often be more than one tune that can account for the behavior. These problems are remedied using carefully constructed selection criteria.

When dealing with the arguments for sines and cosines after a full turn, information about what occurs during the turn will be lost. In the space-charge-free regime there will be no noticeable difference between the orbits with starting tunes

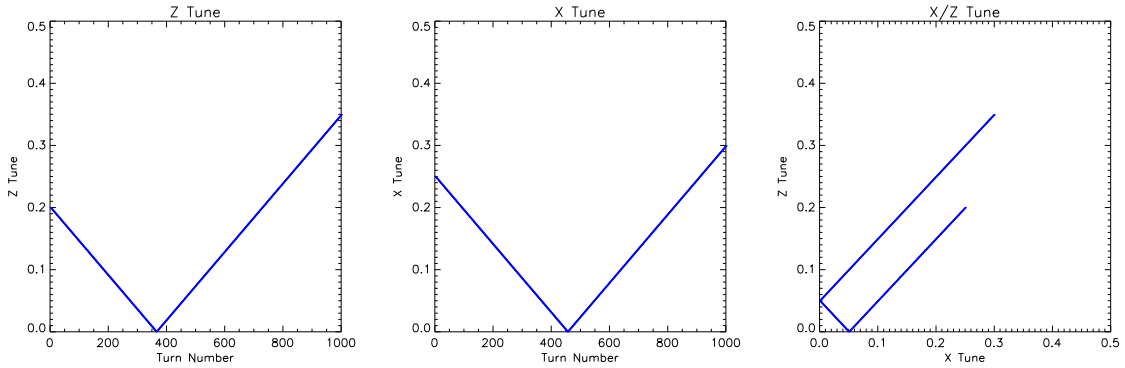

Figure 3.2: Simple tunemap of ramped system.

of 6.25 and those with starting tunes of 4.25. They each have an extra quarter of a revolution after every turn. Thus, when the mapping algorithm searches, all it will find is what fraction of a betatron wavelength has occurred. We can see in the example that the tune loops back on itself, starting at ν_x=0.25 and ν_z=0.20 it moves down to z resonance, over to x resonance, and back up a parallel line (see Fig. 3.2).

Numerous other operations can be performed to view how the tunes change with respect to other variables, which include averaging, binning and statistical analysis.

CHAPTER 4
RESULTS

4.1 Overview

This investigation involved the integration of 5000 test particles that began with a cold beam Gaussian distribution. They were then integrated through 20 different space-charge conditions. Ten conditions dealt with starting betatron-tunes of $\nu_{x0} = 6.25$ and $\nu_{z0} = 6.20$ that were linearly downramped through the whole number resonance. These conditions are referred to as System 1. The other ten dealt with starting betatron-tunes of $\nu_{x0} = 4.25$ and $\nu_{z0} = 4.20$ that were linearly downramped through the whole number resonance. These are referred to as System 2. The relative chaos and regularity of the orbits was then calculated using the patterns method. These systems were chosen since they correspond to experiments performed in Hunag et. al. 2006[2]. Though the exact initial conditions and space-charge values used in their experiments were unknown, the morphology of the orbits and the behavior of the emittance indicated that the model was properly implemented.

We performed a series of analyses using the orbital data and the computed levels of chaos. Quantities such as emittance and betatron-tune were calculated from the data. Furthermore, the evolution of the beam was investigated using individual snapshots of the beam as it evolved through time, as well as individual

orbits which exhibited the behavior that deserved study. Finally, we can use the calculated data along with other values, such as strength of the space-charge kick, to gain a deeper understanding of the roles and causes of chaos in the evolution of the beam for various values of space-charge and betatron-tune.

4.2 Chaos and Beam Size

As stated previously the patterns method has the rare ability to quantify the chaos of a system as it progresses through time. Therefore, in the experiments the chaos of each orbit was calculated for the x dimension. In Figures 4.1 and 4.2 we see the x and z emittances with respect to time plotted along with graphs showing the relative amount of chaos in the beam with respect to time. Since there were 5000 test particles, each one of them being chaotic, sticky or regular, each turn shows a stacked representation of them, blue being the number of particles that are regular, green being the number that are sticky plus the number that are regular, and red being the number that are chaotic plus the number that are sticky plus the number that are regular. This is the reason for the horizontal line at 5000 in each of them. These results are shown in Figures 4.1 and 4.2.

As we move from a no space-charge regime to a high space-charge regime, we see changes in both the relative chaos and the emittance. In the no space-charge regime, the emittance remains at zero. This is to be expected because a cold-beam approximation used here has zero initial emittance, and since there is no space-charge, there is nothing to force the particles outwards and cause emittance growth. As will be seen in Section 4.3, the ensemble of particles merely rotates in trace space. If we look at the chaos distribution, however, there are several

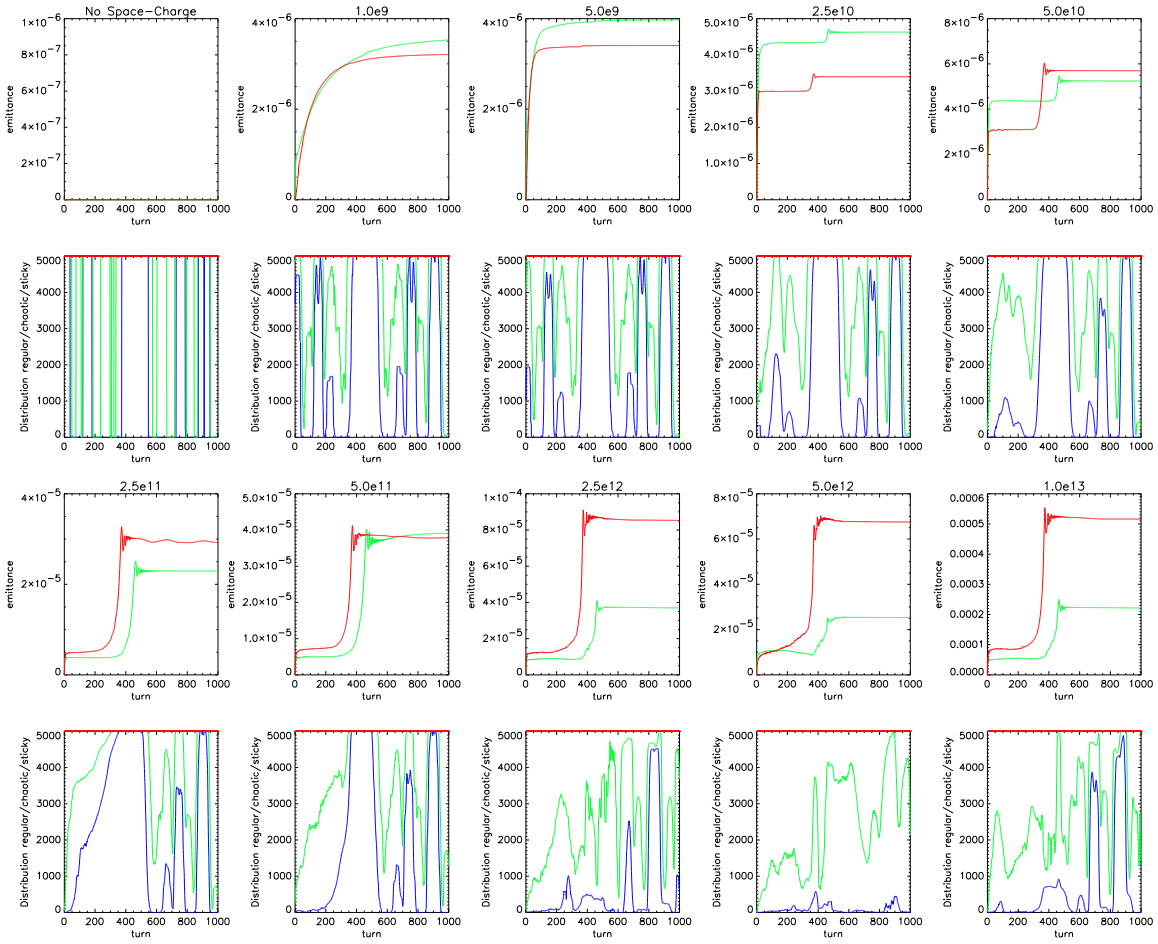

Figure 4.1: SYSTEM 1: For each pair of rows, the top row contains graphs of the trace space emittance in SI units, green being the x dimension and red being the z dimension. The ten different space-charge values used in the study are all represented with the values in particles per meter given at the top. The second row shows a stacked graph of regular, regular + sticky, and regular + sticky + chaotic orbits. This allows a determination of the relative chaos of a system. This graph deals with System 1 – a linearly down-ramped betatron-tune with initial value 6.25 in the x dimension and 6.20 in the z dimension.

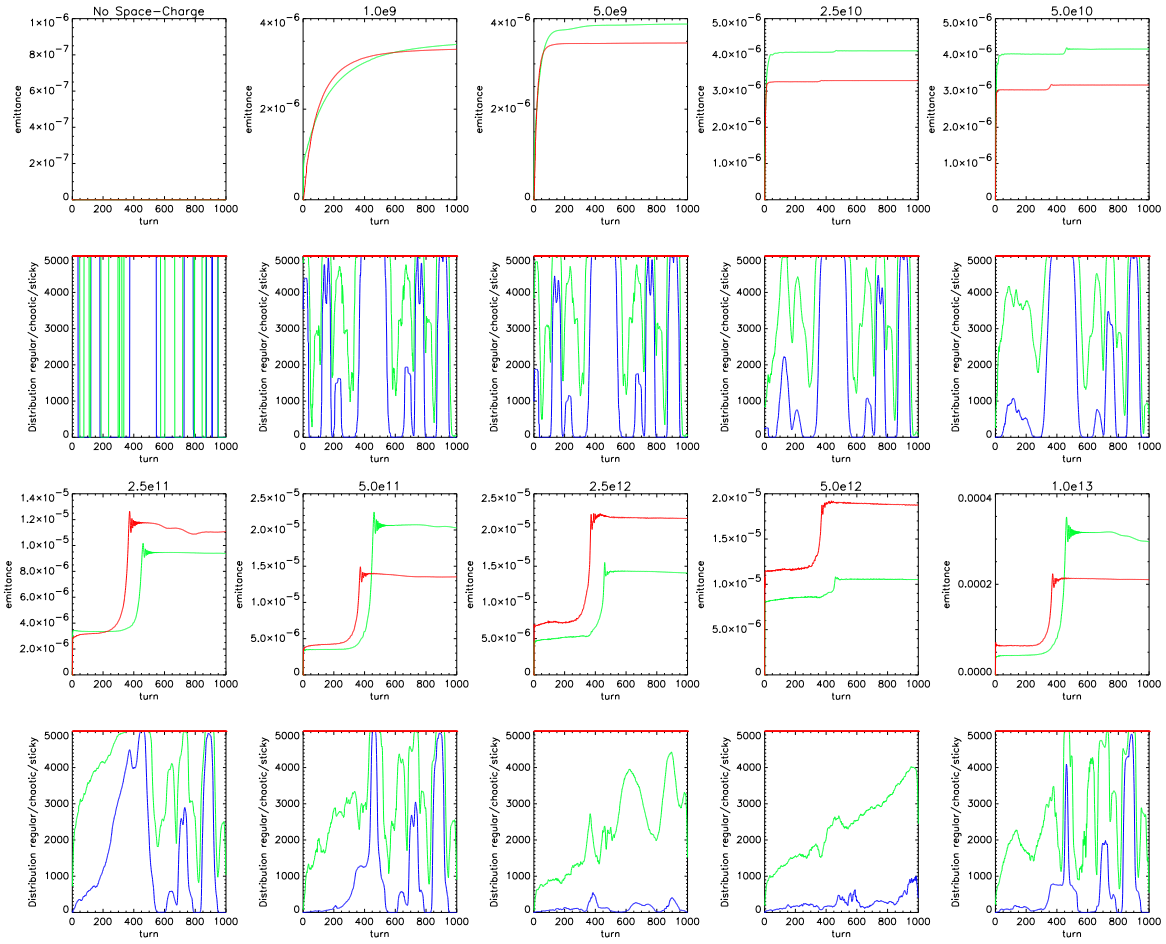

Figure 4.2: SYSTEM 2: For each pair of rows, the top row contains graphs of the trace space emittance in SI units, green being the x dimension and red being the z dimension. The ten different space-charge values used in the study are all represented with the values in particles per meter given at the top. The second row shows a stacked graph of regular, regular + sticky, and regular + sticky + chaotic orbits. This allows a determination of the relative chaos of a system. This graph deals with System 2 – a linearly down-ramped betatron-tune with initial value 4.25 in the x dimension and 4.20 in the z dimension.

distinct chaotic, sticky, and regular epochs. As has been shown in previous research, time dependance by itself can bring about chaos. In this case, there is a changing betatron-tune which will spread out the spectrum of the orbit thus fulfilling one of the conditions of chaos.

The next two space charge regimes are of the order of 10^9 particles per meter. We can see some emittance growth at the beginning, which appears unrelated to the relative chaos graph. This is an artifact of the cold beam approximation – the emittance growth observed is merely phase mixing spreading the beam out while remaining within the trace space ellipse defined by the initial conditions. In the relative chaos plots there are the same epochs of regularity and chaos. However, the beam no longer moves completely between states. There is now a distribution between chaotic, sticky, and regular. The only case where the beam does completely become regular is in the epoch approximately between turns 350 and 550. This epoch contains the point where the linear ramping crosses the whole number resonance in the tune.

In the space-charge regime of the order 10^{10} particles per meter, we see the emergence of a sudden jump in emittance. In this regime the jump is small, between 1 and 3 microns, but it is noticeable. We can see in the graph of relative chaos that while there is further softening of the smaller regular epochs, the resonance condition is still fully regular. Interestingly enough, it directly corresponds to the emittance increase.

When we examine the order of magintude 10^{11} particles per meter, we begin to see not only large scale emittance increases, but significant differences between

System 1 and System 2. While in both systems the chaotic behavior during the period after turn 500 are very similar to the relative chaos of the same periods in lower space-charge regimes, before turn 600 drastic differences show up. We expect the space-charge to have the most impact in this time period because the beam has not significantly grown either in size or velocity. Since the space-charge is inversely proportional to the rms radius and both the cube of the relativistic γ and the square of the velocity, the space-charge will be at its strongest here. The regular peaks that appeared before resonance in the lower space-charge regimes now have either become sticky or been absorbed into the resonance condition. The absorbtion phenomenon is most prevalent in System 1, while in the other system this phenomenon is only widely seen in the 2.5×10^{11} regime. While in System 1 there is still a large entirely regular epoch surrounding the resonance condition, in System 2 this has been drastically shortened with a much larger spread of relative chaos throughout.

The space-charge regime of order 10^{12} is where things truly become interesting: the chaos distributions for the two betatron-tune systems could not be more different. In the 2.5×10^{12} regime System 1, after turn 600, behaves similar to the lower space-charge regimes, while in System 2 this behavior is nonexistent. In both systems, the number of chaotic orbits is high, but there are in all four examples a small number of orbits that still appear to show resonance.

Finally, in the 10^{13} particles per meter regime, we actually see a return to what appears to be the type of chaos distributions lower space-charge epochs experience. We can see in System 1 that the relative chaos returns to the same distribution as

lower space-charge after turn 600. Furthermore the chaos distribution for System 2 looks a great deal like the distribution for the 5×10^{11} regime.

Close examination of these plots brings up two concerns that seem to go against our intuition. First, why does the emittance in both systems begin to decrease after the 5×10^{11} regime before drastically increasing in the 1×10^{13} regime? Second, why does the relative chaos abandon its shape before having it reappear in the 1×10^{13} regime?

Investigations of these phenomena will continue and will show that the answer to both of these questions comes from the way that orbits expand in the various space-charge regimes, as well as the effect space-charge has on the betatron-tune of the beam.

4.3 Trace-Space Slices

In this experiment we have taken cross sections of the beam and watched how they evolved. It will be found that this experiment will shed light on the reasons for the strange behavior of the emittance in the high space-charge regime. Each plot shows ten slices for each system, the first slice being taken at turn 100 then increasing at intervals of 100 until reaching the end at 1000. The results are shown in Figures 4.3 through 4.12.

The no space-charge regime in both betatron-tune systems is shown in Figure 4.3. Here we can see why the emittance remains at zero: the initial conditions remain in a line rotating through trace-space.

When space-charge is introduced, we can see that its position dependence will smear out the line in which the beam was initially and turn it into a spiral that

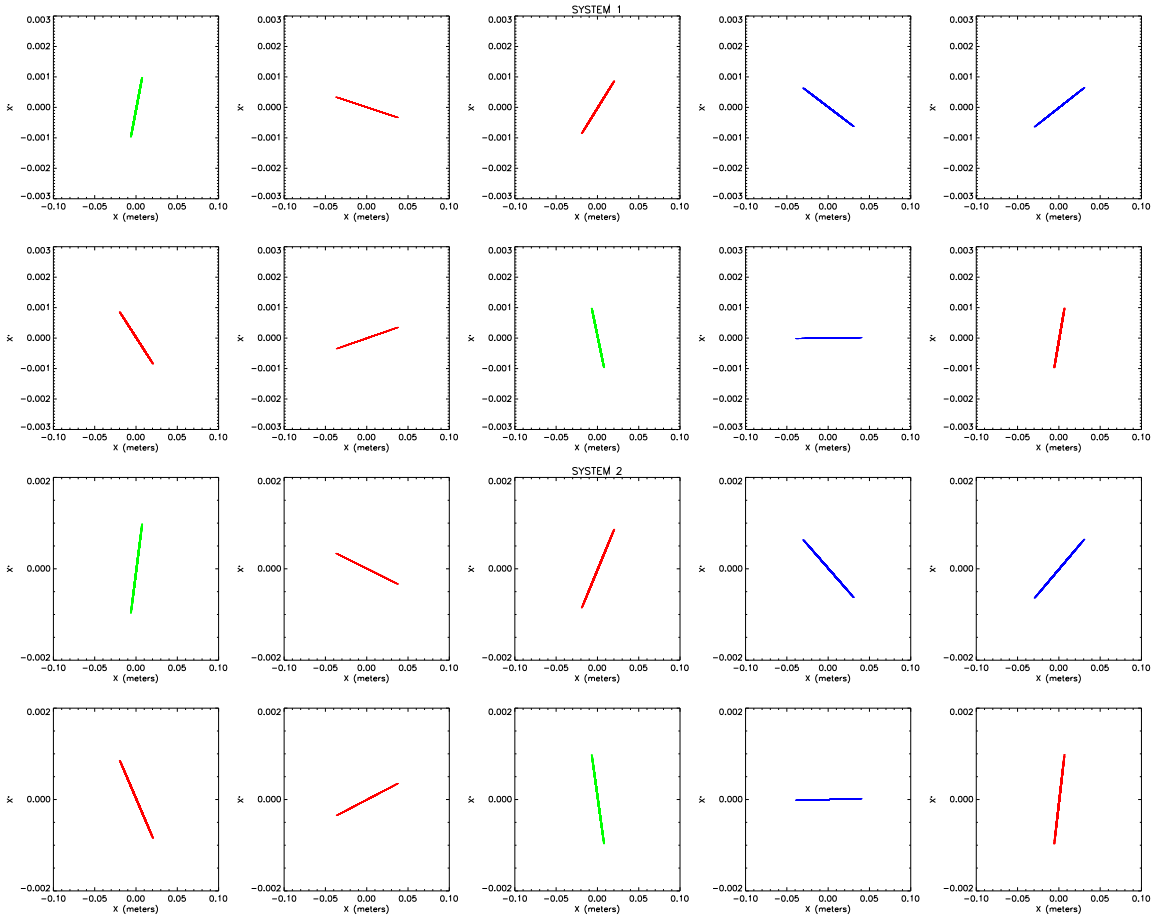

Figure 4.3: Trace-space projections (x v. x') of the beam at various times starting at 100 turns and moving to 1000 turns. This is the no space-charge regime. Red denotes chaotic orbits, green sticky and blue regular.

rotates, but does not grow in trace-space. This is true in the 1×10^9 and 5×10^9 regimes for both systems investigated in this study. They are plotted in Figures 4.4 and 4.5.

Once the 10^{10} regime has been reached, we expect to see some small emittance growth. This is confirmed in Figures 4.6 through 4.7, where we can even see the

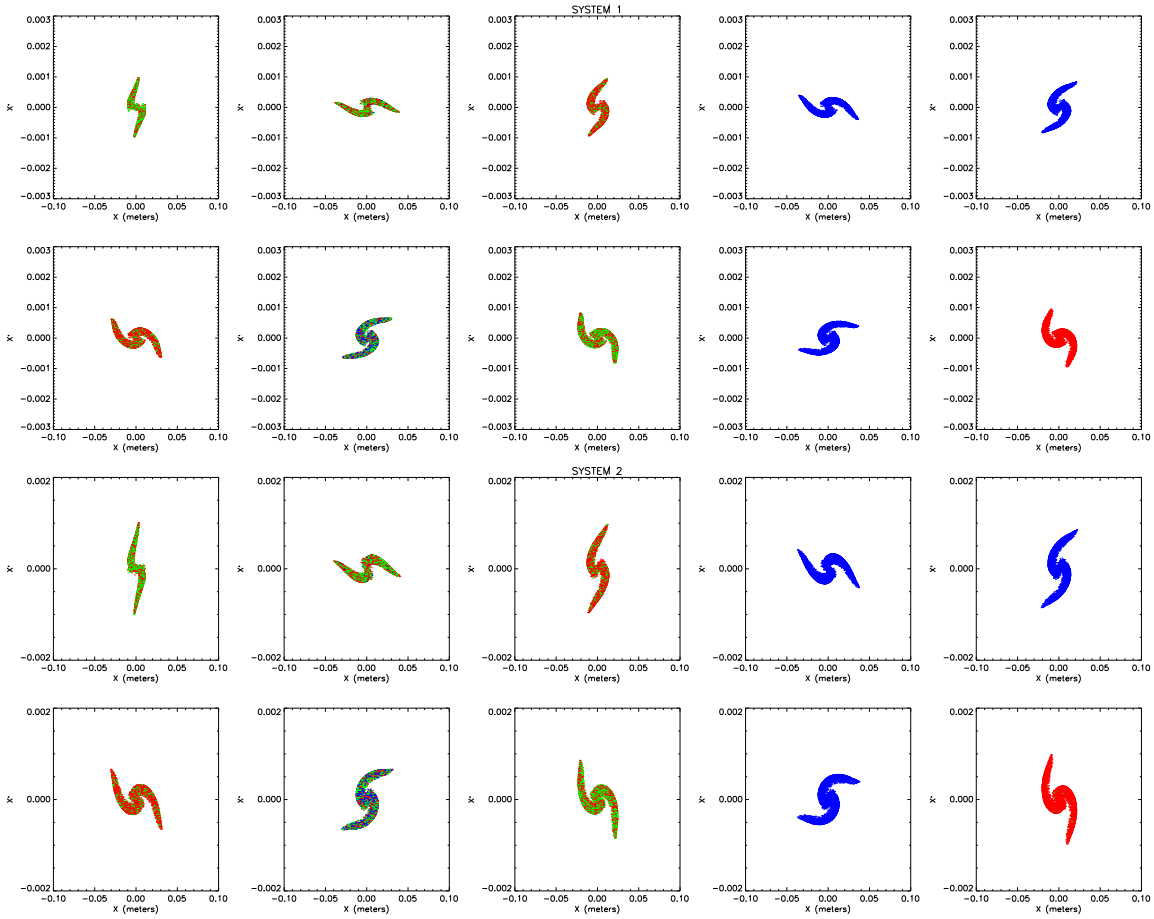

Figure 4.4: Trace-space projections (x v. x') of the beam at various times starting at 100 turns and moving to 1000 turns for System 1 (top two rows) and System 2 (bottom two rows). This is the 1×10^9 particles per meter space-charge regime. Red denotes chaotic orbits, green sticky and blue regular.

beginning of islands forming around the periphery of the beam.

As we enter the higher space-charge regimes, particularly the 2.5×10^{11} and 5×10^{11} regimes, we can begin to see the mechanisms for emittance growth. The resonance condition should occur approximately around turn 400 and we can see in

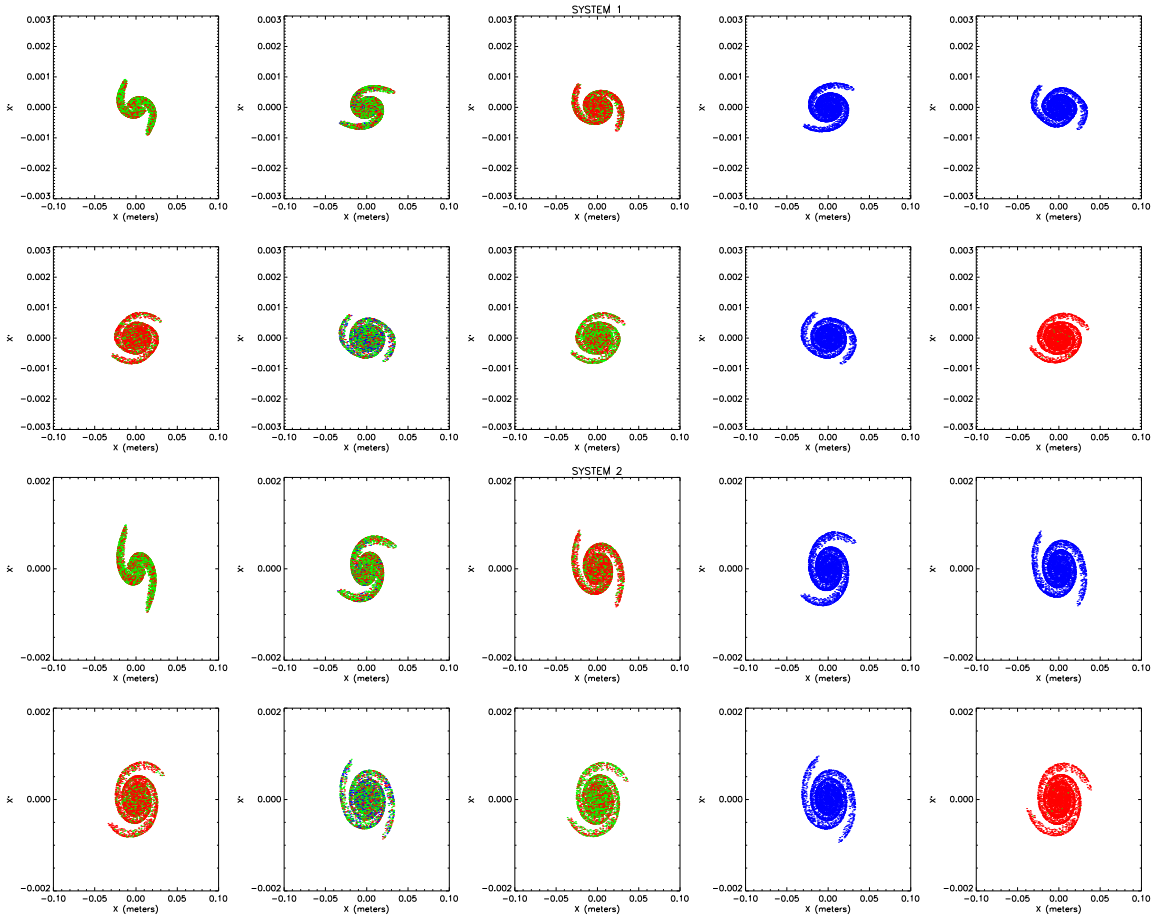

Figure 4.5: Trace-space projections (x v. x') of the beam at various times starting at 100 turns and moving to 1000 turns for System 1 (top two rows) and System 2 (bottom two rows). This is the 5×10^9 particles per meter space-charge regime. Red denotes chaotic orbits, green sticky and blue regular.

Figures 4.8 and 4.9 that the growth of the beam occurs between turn 300 and turn 500, evolving from a beam with small islands into one with a large halo.

Now that the higher space-charge regimes have been reached ($> 10^{12}$ particles per meter), things become difficult to read. The results for these regimes are shown

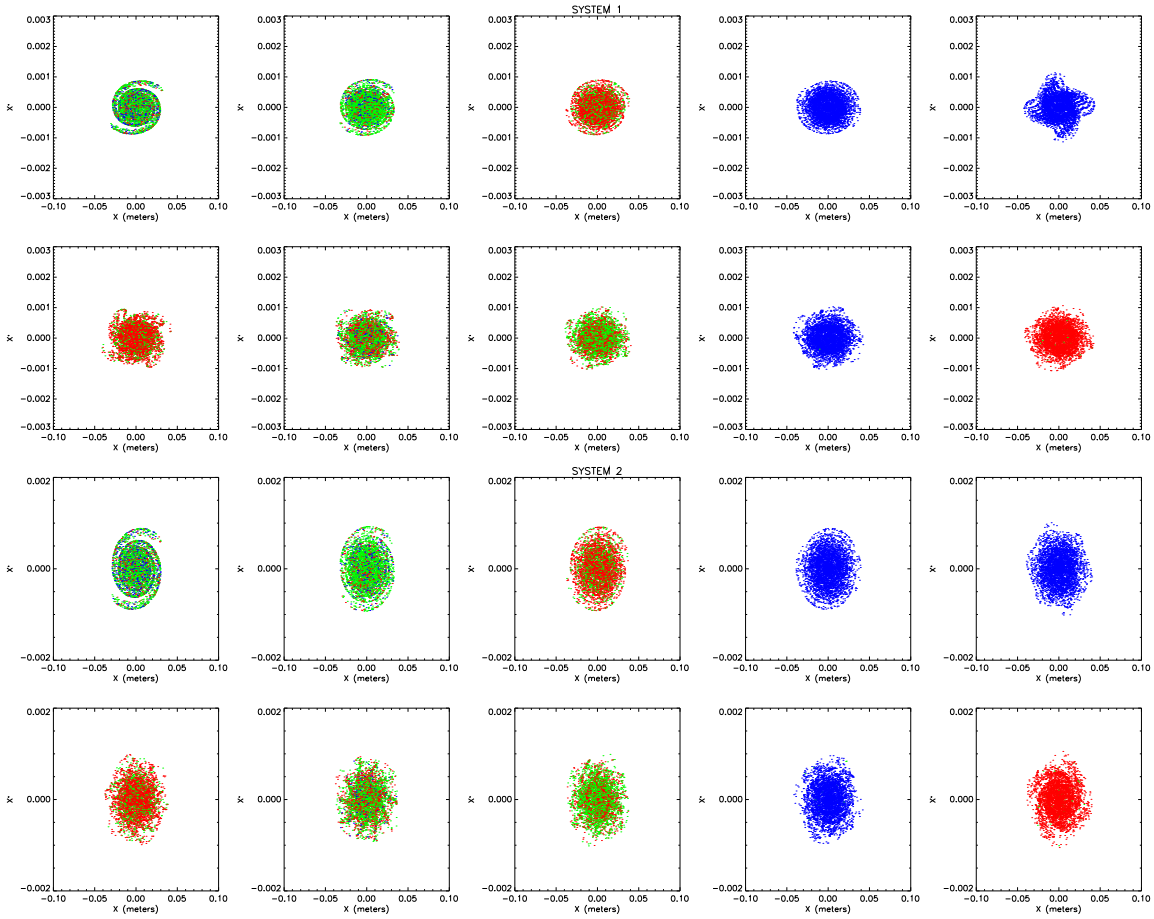

Figure 4.6: Trace-space projections (x v. x') of the beam at various times starting at 100 turns and moving to 1000 turns for System 1 (top two rows) and System 2 (bottom two rows). This is the 2.5×10^{10} particles per meter space-charge regime. Red denotes chaotic orbits, green sticky and blue regular.

in Figures 4.10 and 4.11. Instead of islands expanding and being smeared into a halo as was seen in lower space charge regimes, these act more like clouds forming around the central beam. We can see why the emittance growth is not as large: since the majority of the particles stay within a small area and only a diffuse cloud

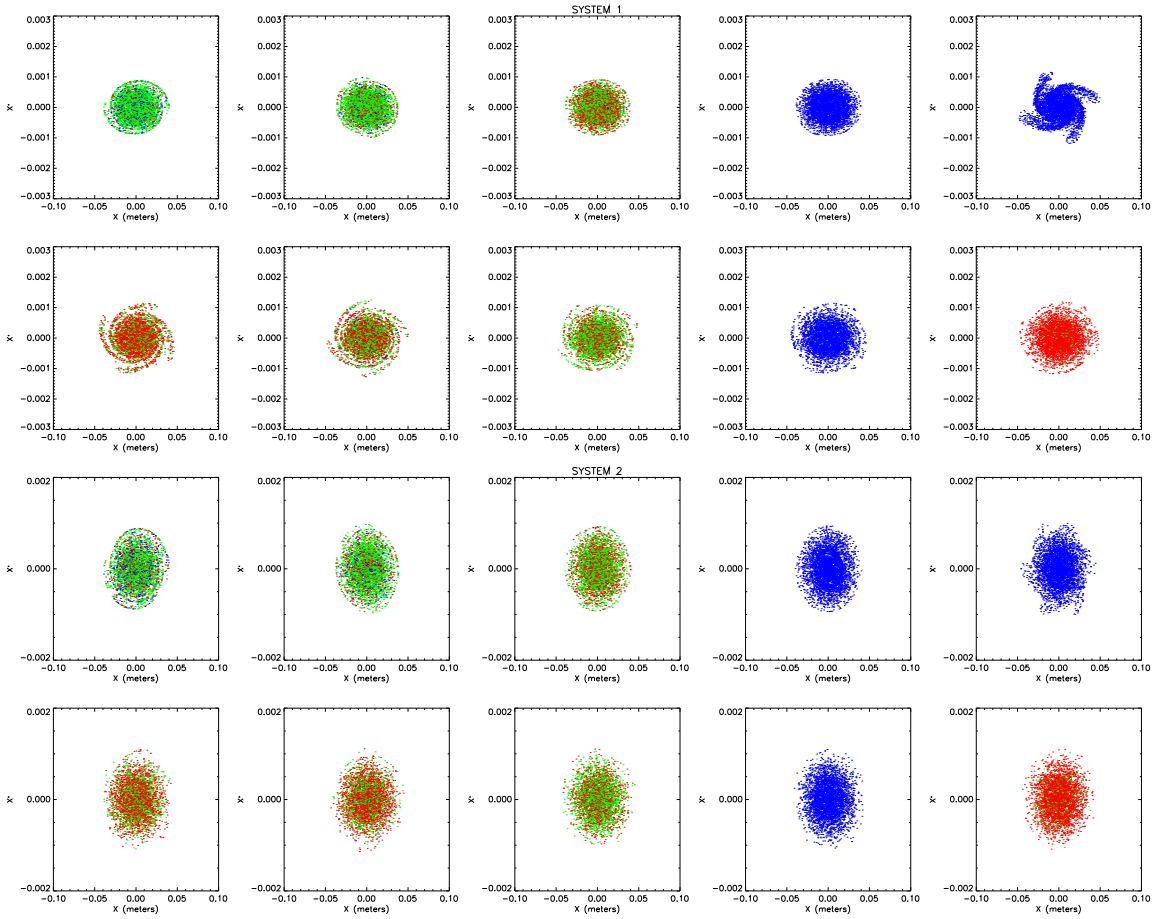

Figure 4.7: Trace-space projections (x v. x') of the beam at various times starting at 100 turns and moving to 1000 turns for System 1 (top two rows) and System 2 (bottom two rows). This is the 5×10^{10} particles per meter space-charge regime. Red denotes chaotic orbits, green sticky and blue regular.

expands. The emittance, which is based on the average square of the distance from the center, remains small even as particles expand to large distances from the center.

The 10^{13} regime is different from the 10^{12} regime in that it again takes on a more ordered expansion, almost like an average between the 10^{11} and 10^{12} regimes.

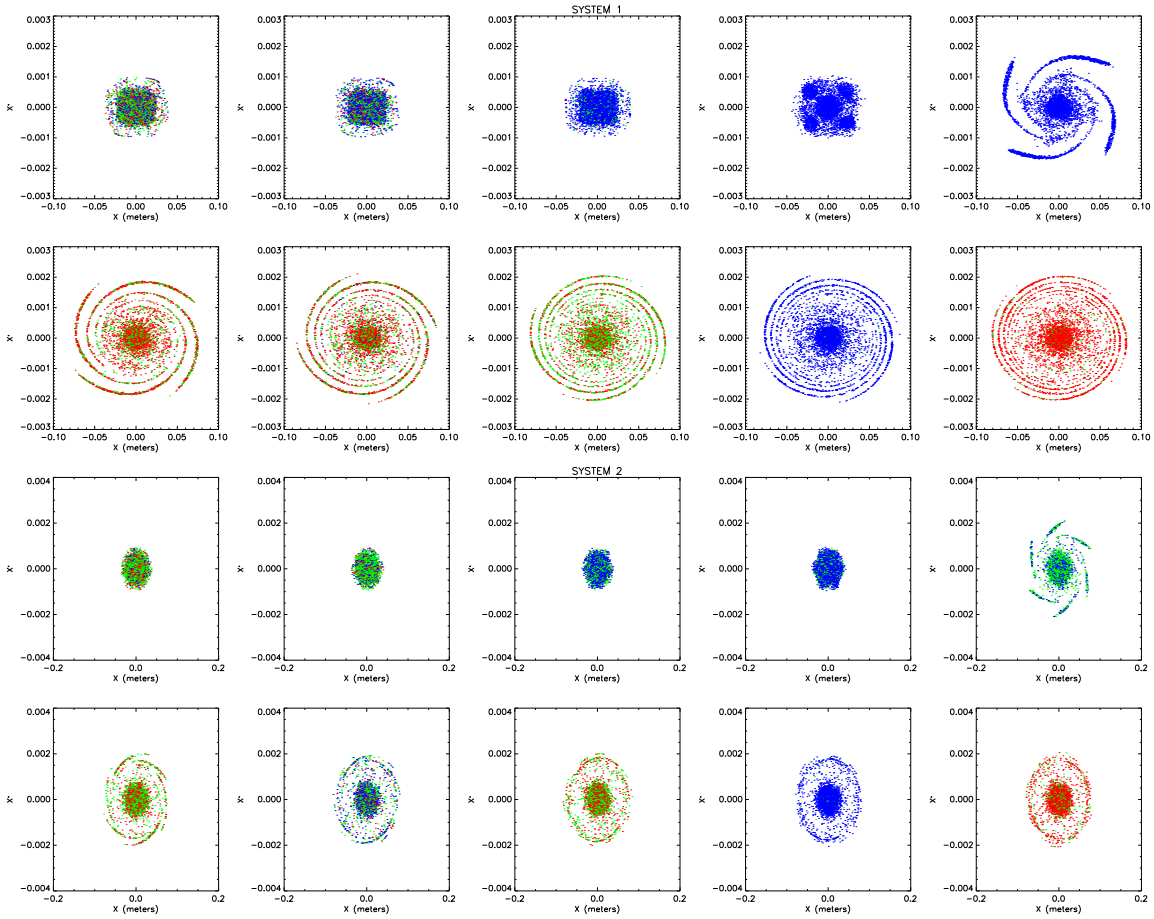

Figure 4.8: Trace-space projections (x v. x') of the beam at various times starting at 100 turns and moving to 1000 turns for System 1 (top two rows) and System 2 (bottom two rows). This is the 2.5×10^{11} particles per meter space-charge regime. Red denotes chaotic orbits, green sticky and blue regular.

There are definite islands that are pulled out, though they are not as strongly defined as before. This is another example of the regression that occurs in the 10^{13} regime.

An answer may be found in the fact that this regime covers a much larger area. In the model used here, the space-charge force drops off exponentially; at a

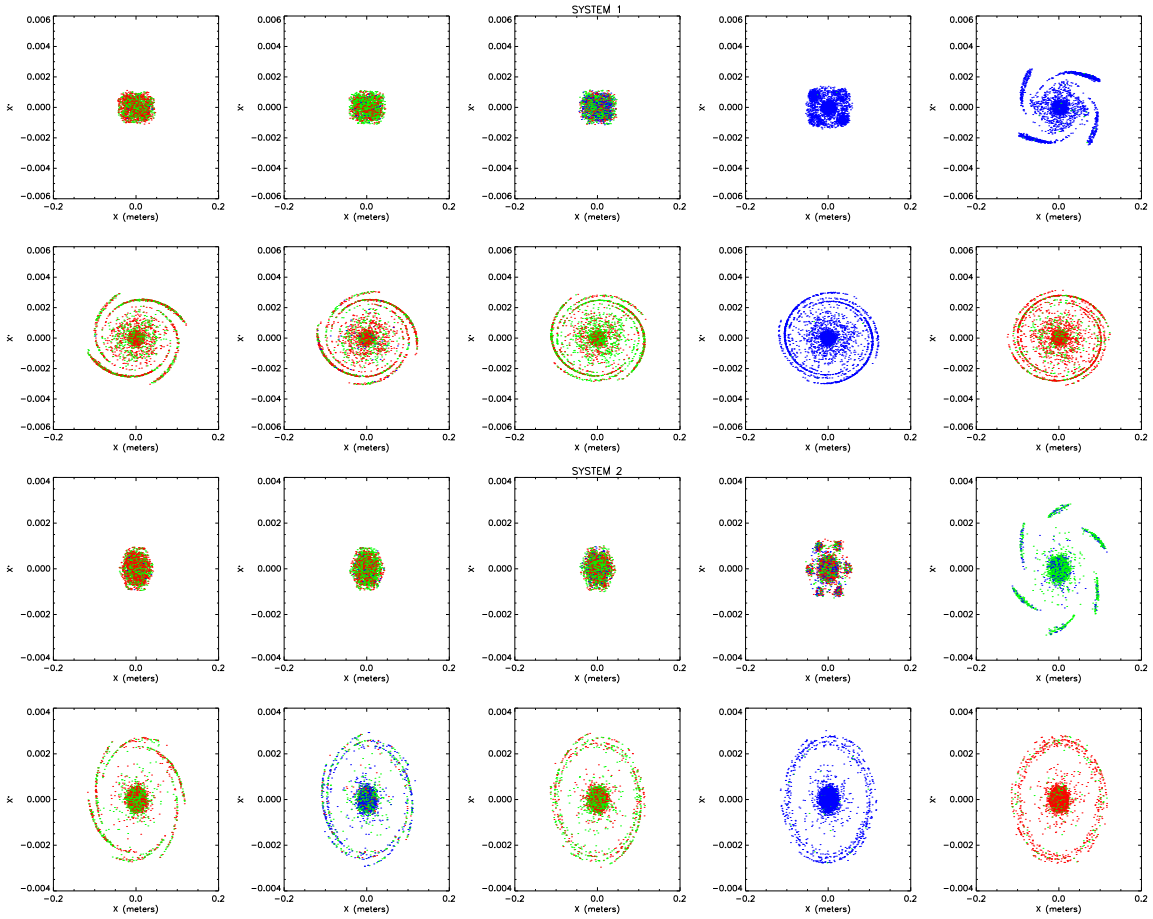

Figure 4.9: Trace-space projections (x v. x') of the beam at various times starting at 100 turns and moving to 1000 turns for System 1 (top two rows) and System 2 (bottom two rows). This is the 5×10^{11} particles per meter space-charge regime. Red denotes chaotic orbits, green sticky and blue regular.

certain point the space-charge force will have reduced to the point that the beam's particles will act as though they are in a smaller space-charge regime.

With these plots we are closer to seeing how the beam evolves through time. We can see how the drastic changes in emittance with respect to space-charge occur,

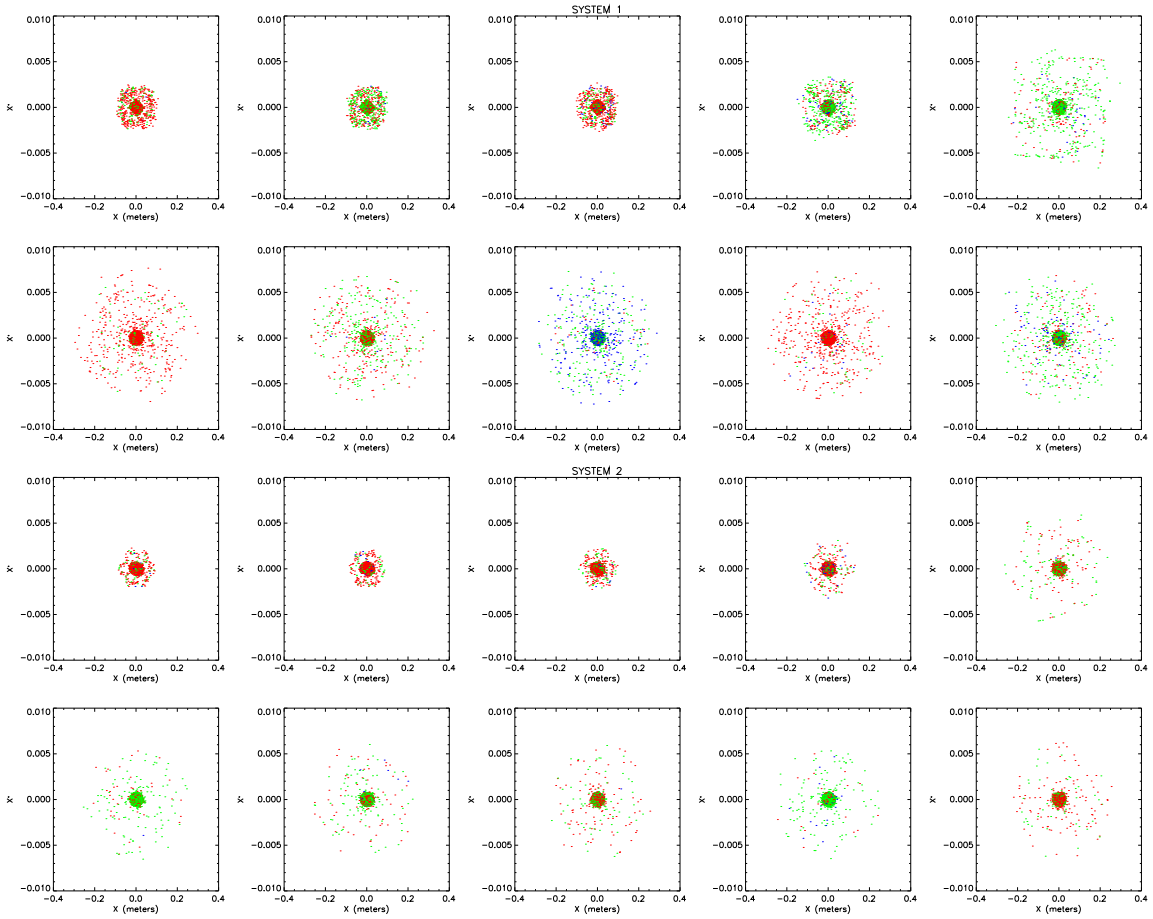

Figure 4.10: Trace-space projections (x v. x') of the beam at various times starting at 100 turns and moving to 1000 turns for System 1 (top two rows) and System 2 (bottom two rows). This is the 2.5×10^{12} particles per meter space-charge regime. Red denotes chaotic orbits, green sticky and blue regular.

and have received hints as to what is happening. We have seen from the emittance and the plots for the highest space-charge regime that what might be occurring involves a reduction in space-charge.

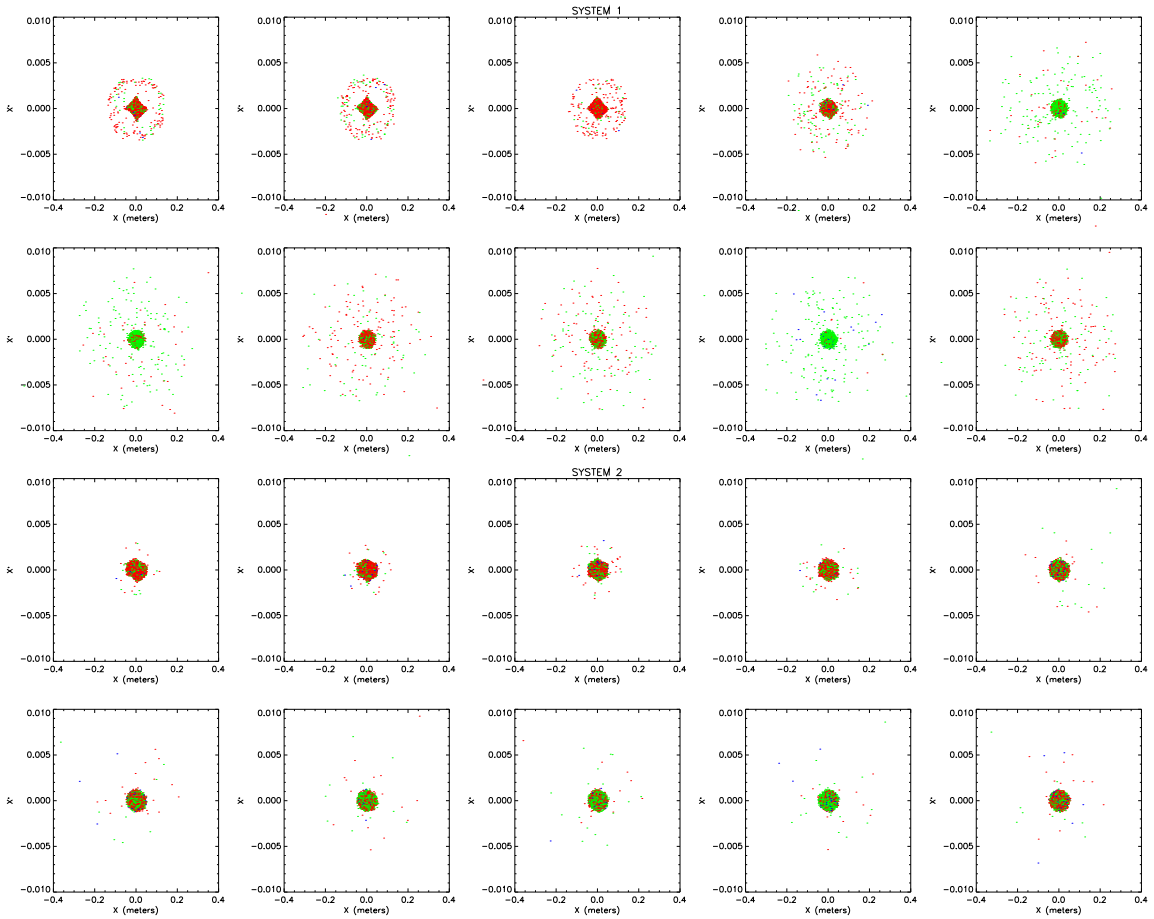

Figure 4.11: Trace-space projections (x v. x') of the beam at various times starting at 100 turns and moving to 1000 turns for System 1 (top two rows) and System 2 (bottom two rows). This is the 5×10^{12} particles per meter space-charge regime. Red denotes chaotic orbits, green sticky and blue regular.

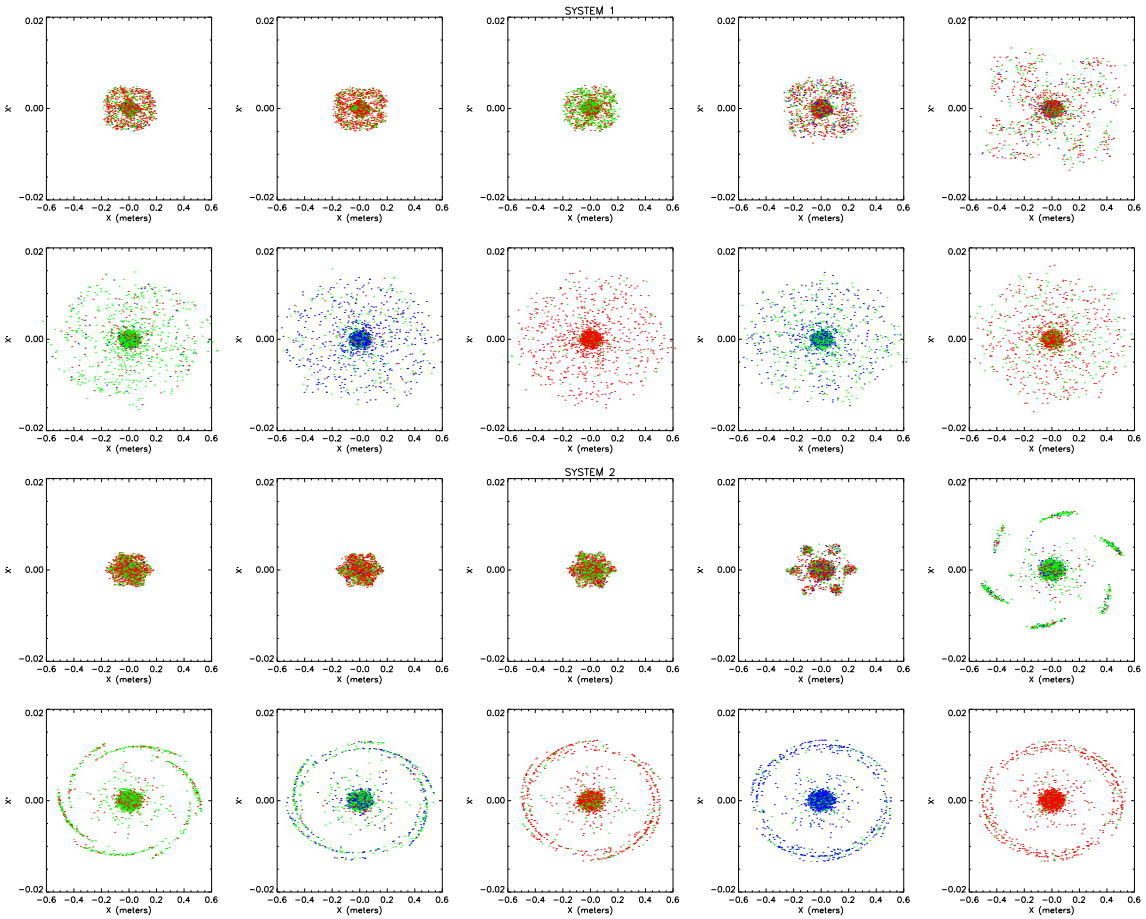

Figure 4.12: Trace-space projections (x v. x') of the beam at various times starting at 100 turns and moving to 1000 turns for System 1 (top two rows) and System 2 (bottom two rows). This is the 1×10^{13} particles per meter space-charge regime. Red denotes chaotic orbits, green sticky and blue regular.

Since we see different behavior at the 300, 400, and 500 turn slices in the 10^{12} regime than in the others, we might question whether resonance is occurring. In order to fully understand the mechanisms behind emittance growth, we will look more closely at the epoch where the growth occurs. Since emittance change begins with the 10^{10} regime, we will start with that. A cursory look shows us that we need only look at the space between turns 400 and 500. The results of this expansion are shown in Figures 4.13 through 4.14. While these do show some island expansion, it is very small.

For the regimes with space charge larger that 10^{11} the slices taken previously seemed to show that the period between turn 300 and turn 400 was also interesting. Henceforth, the slices will examine the period between turn 300 and turn 500. Here we see what we were expecting: the islands form, get pulled outwards as resonance occurs, and are then smeared into a halo. The results are shown in Figures 4.15 through 4.24.

There are several differences between the 2.5×10^{12} and the 5×10^{12} regimes. In the lower space-charge regime, we still see some of the progression present in the 10^{11} regime, while in the higher space-charge regime we do not. In Figures 4.19 and 4.20 we can see how very blurry islands form and spread outwards before being completely washed away.

In Figures 4.21 and 4.22, there is no orderly progression, nor are there any islands. All that shows up is a steadily growing cloud of particles.

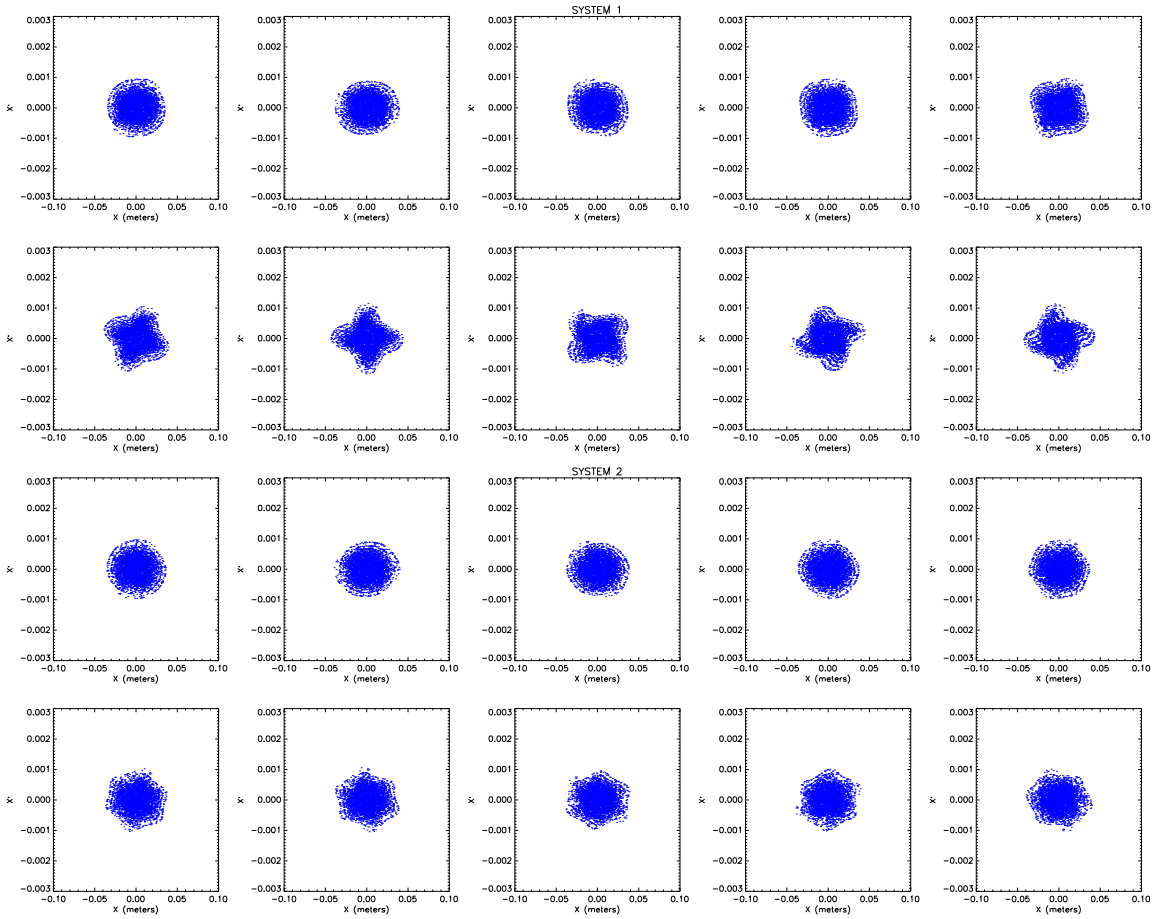

Figure 4.13: Trace-space projections (x v. x') of the beam at various times starting at 410 turns and moving to 500 turns for System 1 (top two rows) and System 2 (bottom two rows). This area shows the emittance growth of the beam, and has been investigated to watch this increase in detail. This is the 2.5×10^{10} particles per meter space-charge regime. Red denotes chaotic orbits, green sticky and blue regular.

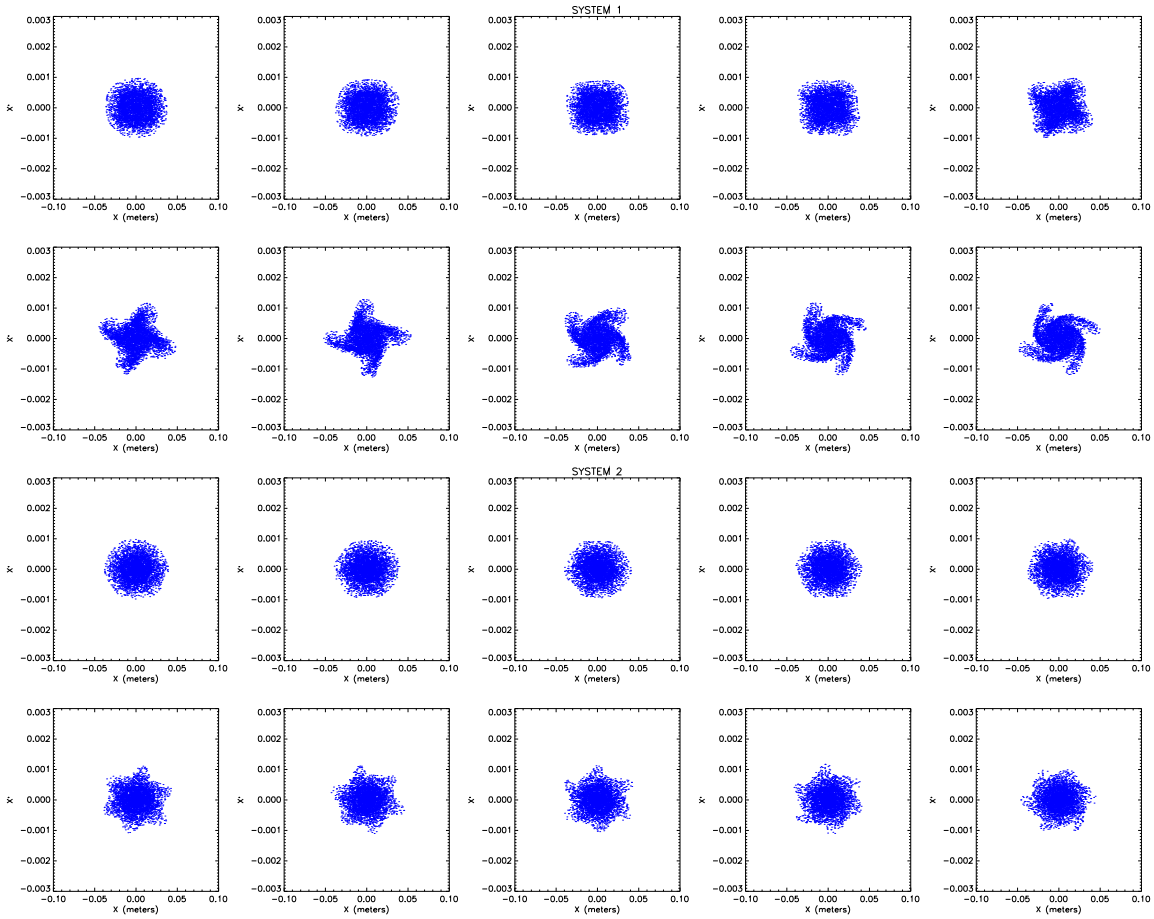

Figure 4.14: Trace-space projections (x v. x') of the beam at various times starting at 410 turns and moving to 500 turns for System 1 (top two rows) and System 2 (bottom two rows). This area shows the emittance growth of the beam, and has been investigated to watch this increase in detail. This is the 5×10^{10} particles per meter space-charge regime. Red denotes chaotic orbits, green sticky and blue regular.

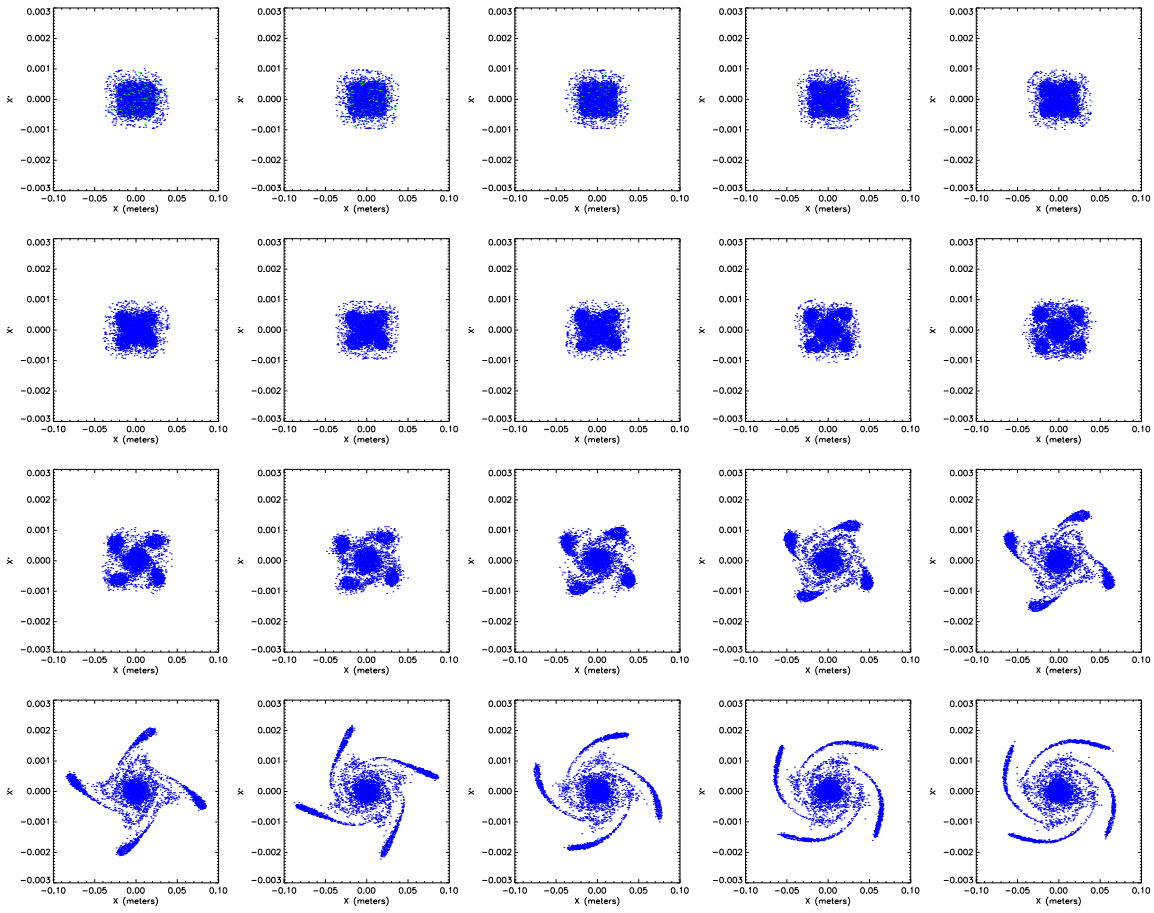

Figure 4.15: SYSTEM 1: Trace-space projections (x v. x') of the beam at various times starting at 310 turns and moving to 500 turns. This area shows the emittance growth of the beam, and has been investigated to watch this increase in detail. This is the 2.5×10^{11} particles per meter space-charge regime. Red denotes chaotic orbits, green sticky and blue regular.

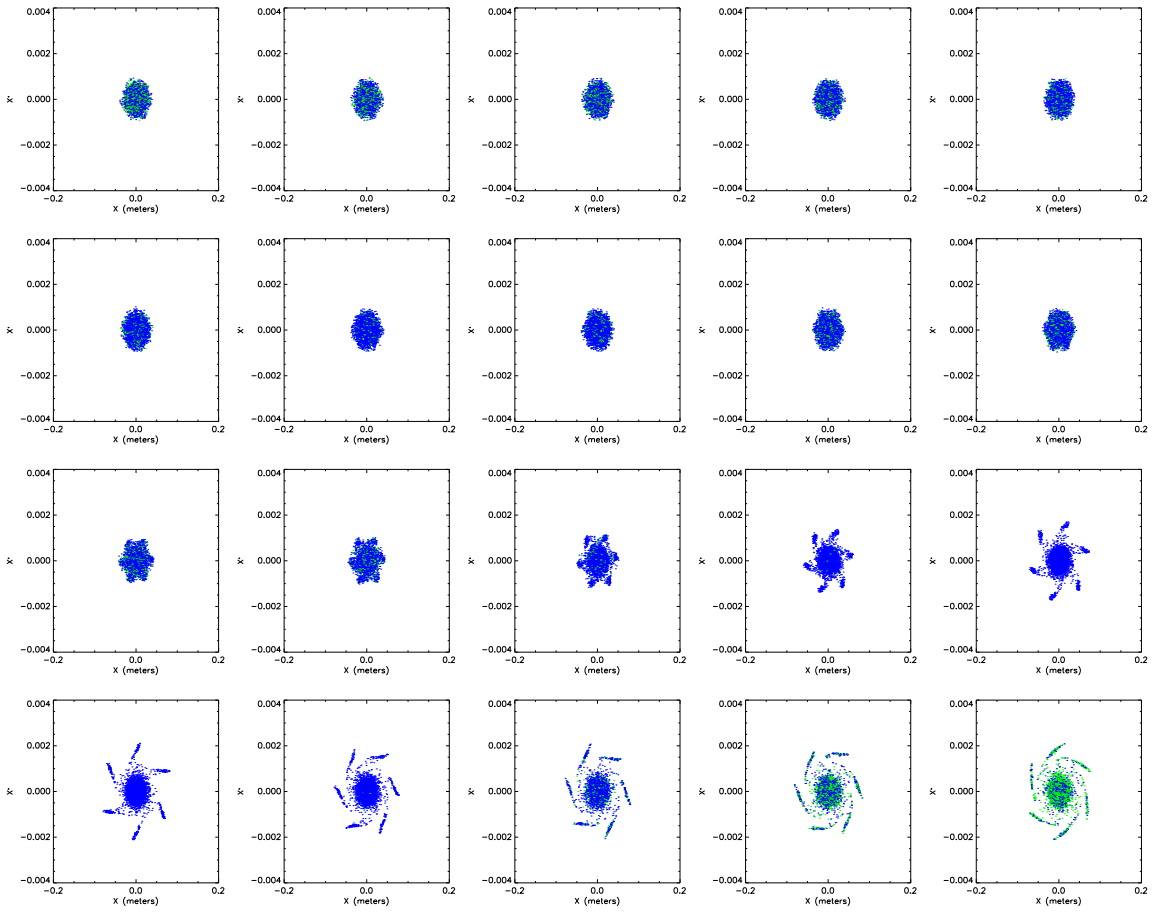

Figure 4.16: SYSTEM 2: Trace-space projections (x v. x') of the beam at various times starting at 310 turns and moving to 500 turns. This area shows the emittance growth of the beam, and has been investigated to watch this increase in detail. This is the 2.5×10^{11} particles per meter space-charge regime. Red denotes chaotic orbits, green sticky and blue regular.

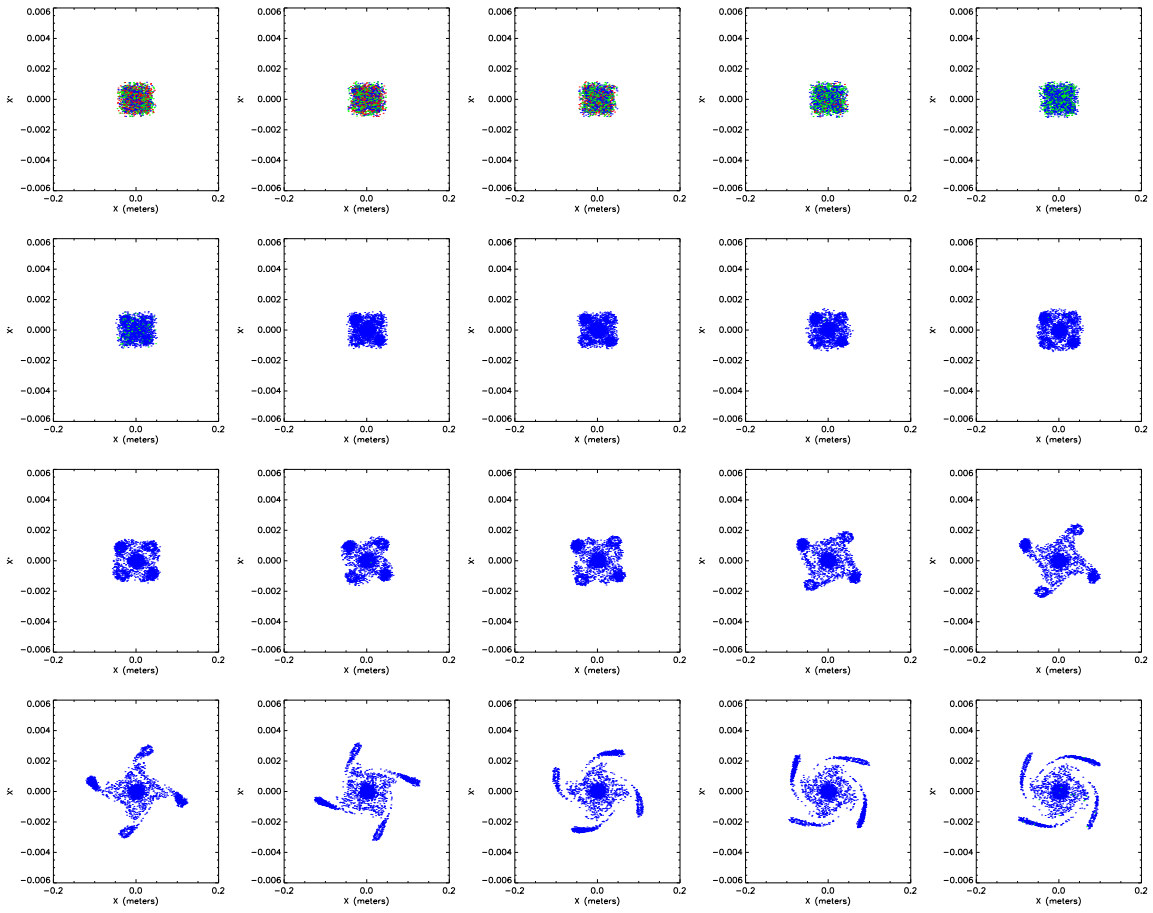

Figure 4.17: SYSTEM 1: Trace-space projections (x v. x') of the beam at various times starting at 310 turns and moving to 500 turns. This area shows the emittance growth of the beam, and has been investigated to watch this increase in detail. This is the 5×10^{11} particles per meter space-charge regime. Red denotes chaotic orbits, green sticky and blue regular.

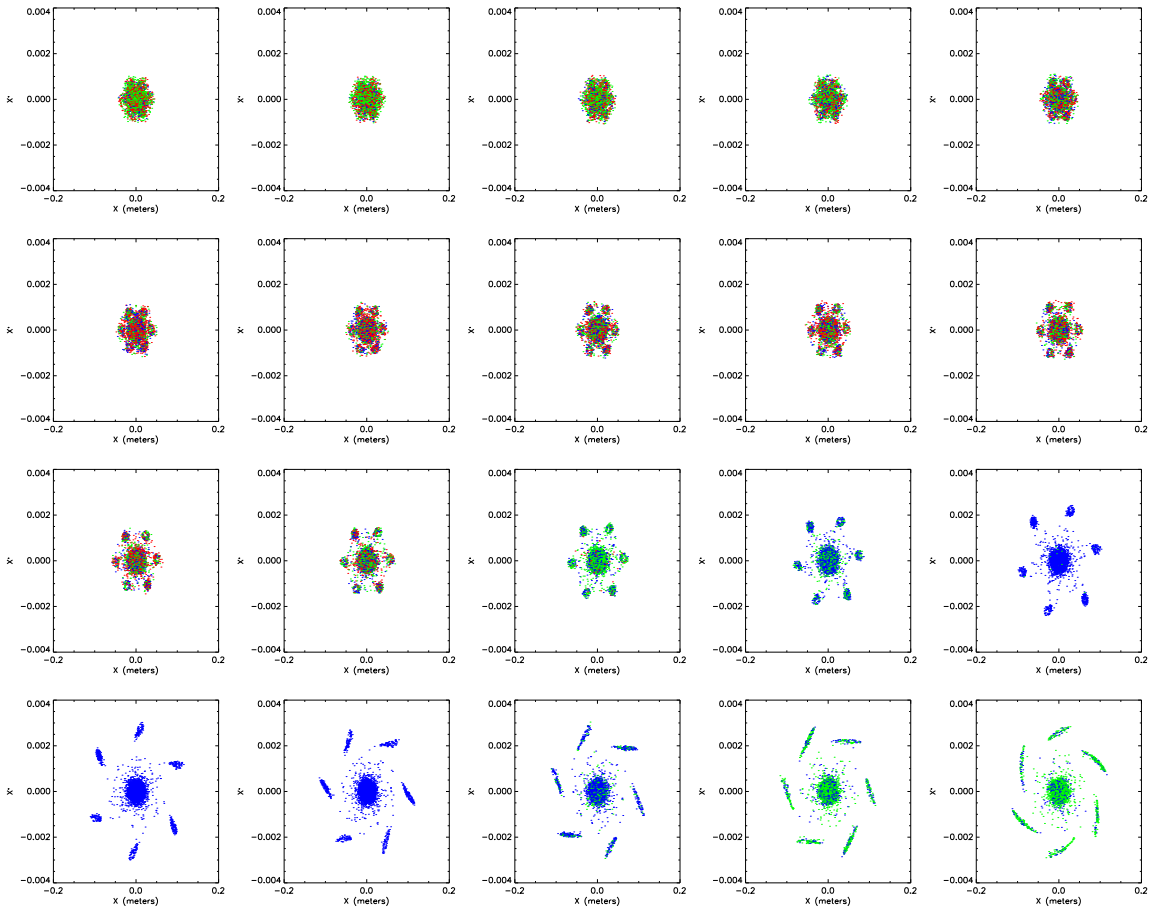

Figure 4.18: SYSTEM 2: Trace-space projections (x v. x') of the beam at various times starting at 310 turns and moving to 500 turns. This area shows the emittance growth of the beam, and has been investigated to watch this increase in detail. This is the 5×10^{11} particles per meter space-charge regime. Red denotes chaotic orbits, green sticky and blue regular.

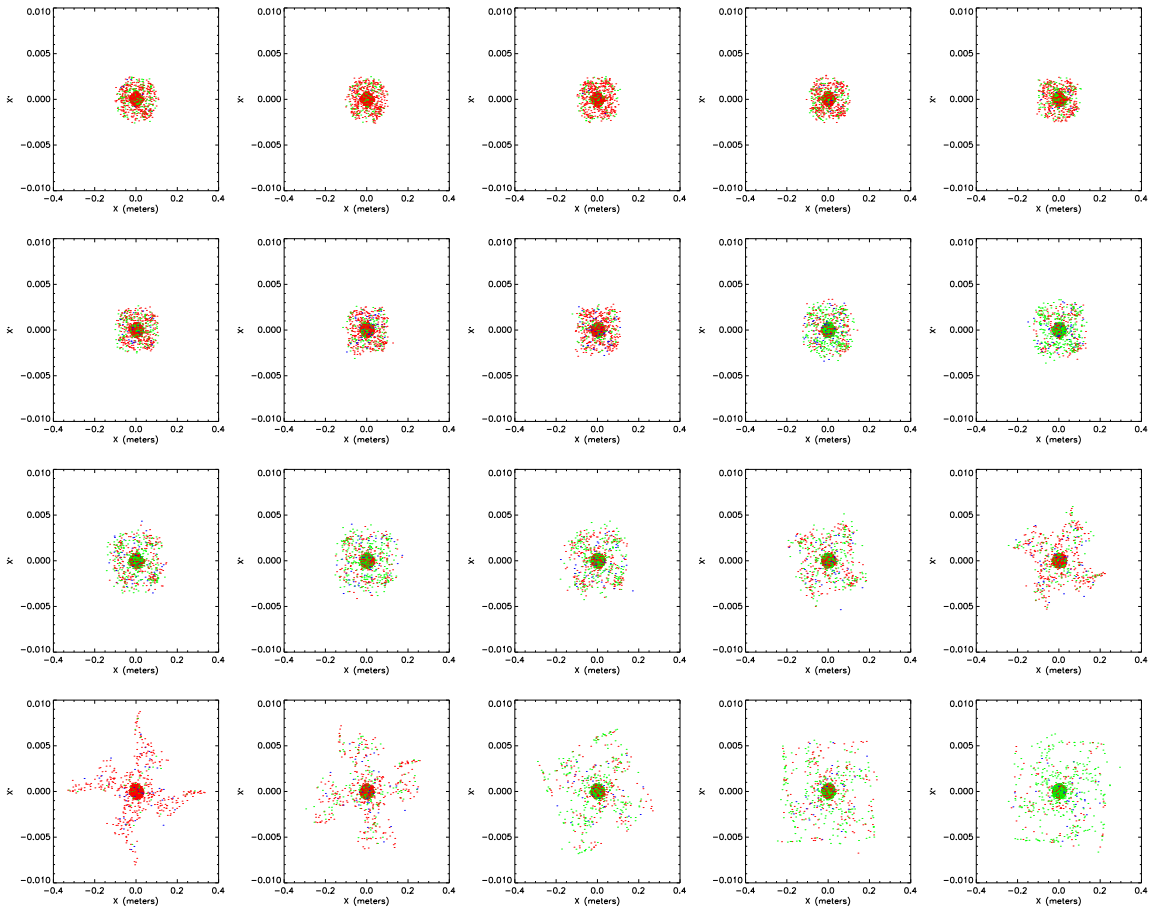

Figure 4.19: SYSTEM 1: Trace-space projections (x v. x') of the beam at various times starting at 310 turns and moving to 500 turns. This area shows the emittance growth of the beam, and has been investigated to watch this increase in detail. This is the 2.5×10^{12} particles per meter space-charge regime. Red denotes chaotic orbits, green sticky and blue regular.

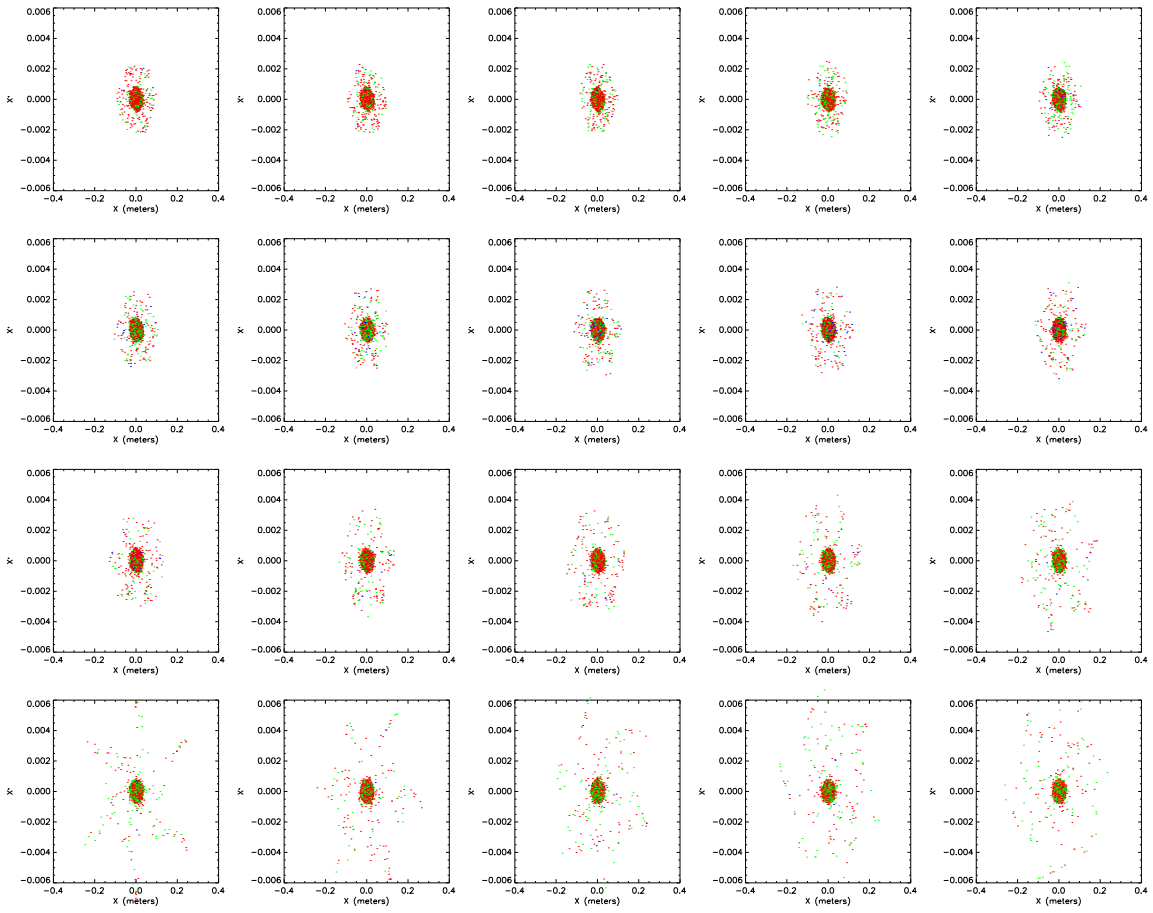

Figure 4.20: SYSTEM 2: Trace-space projections (x v. x') of the beam at various times starting at 310 turns and moving to 500 turns. This area shows the emittance growth of the beam, and has been investigated to watch this increase in detail. This is the 2.5×10^{12} particles per meter space-charge regime. Red denotes chaotic orbits, green sticky and blue regular.

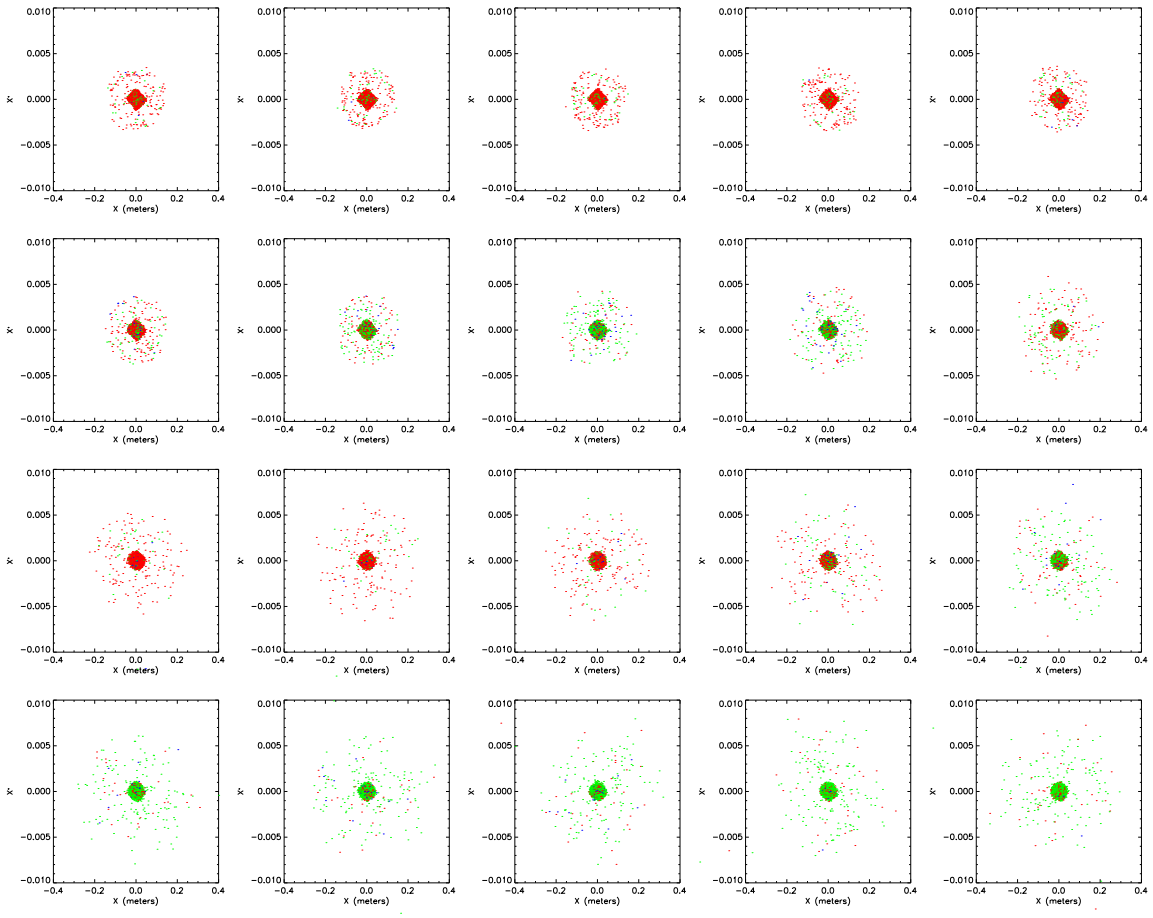

Figure 4.21: SYSTEM 1: Trace-space projections (x v. x') of the beam at various times starting at 310 turns and moving to 500 turns. This area shows the emittance growth of the beam, and has been investigated to watch this increase in detail. This is the 5×10^{12} particles per meter space-charge regime. Red denotes chaotic orbits, green sticky and blue regular.

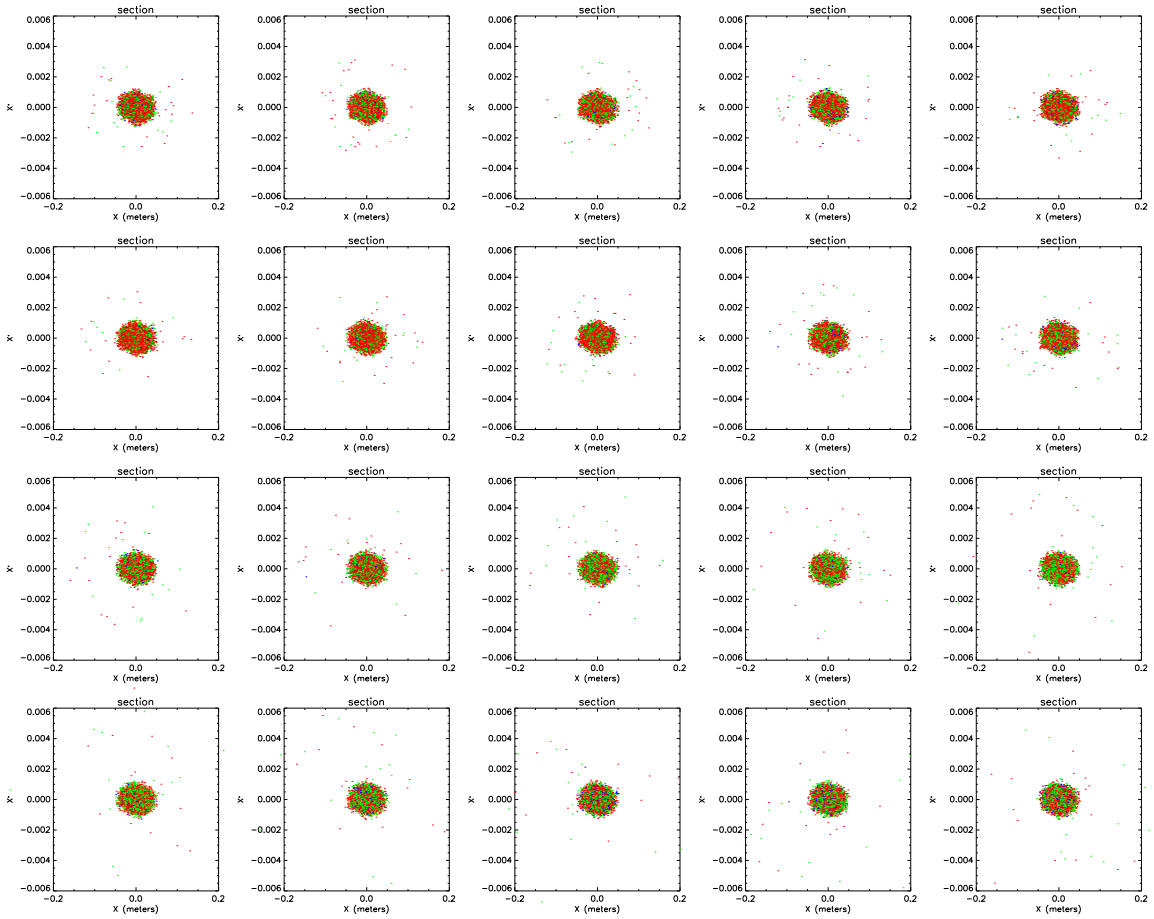

Figure 4.22: SYSTEM 2: Trace-space projections (x v. x') of the beam at various times starting at 310 turns and moving to 500 turns. This area shows the emittance growth of the beam, and has been investigated to watch this increase in detail. This is the 5×10^{12} particles per meter space-charge regime. Red denotes chaotic orbits, green sticky and blue regular.

In the final set of slices, we look at the largest of the space-charge regimes. An orderly progression with islands forming, being pulled out, then smeared into a halo can be seen in Figures 4.23 and 4.24. It is interesting to note that the only real resonance-type phenomenon, where nearly the entire beam becomes regular,

occurrs in System 2, as was shown in Figure 4.2. However, the expansion in Figure 4.23 happens even with a large number of the orbits being chaotic.

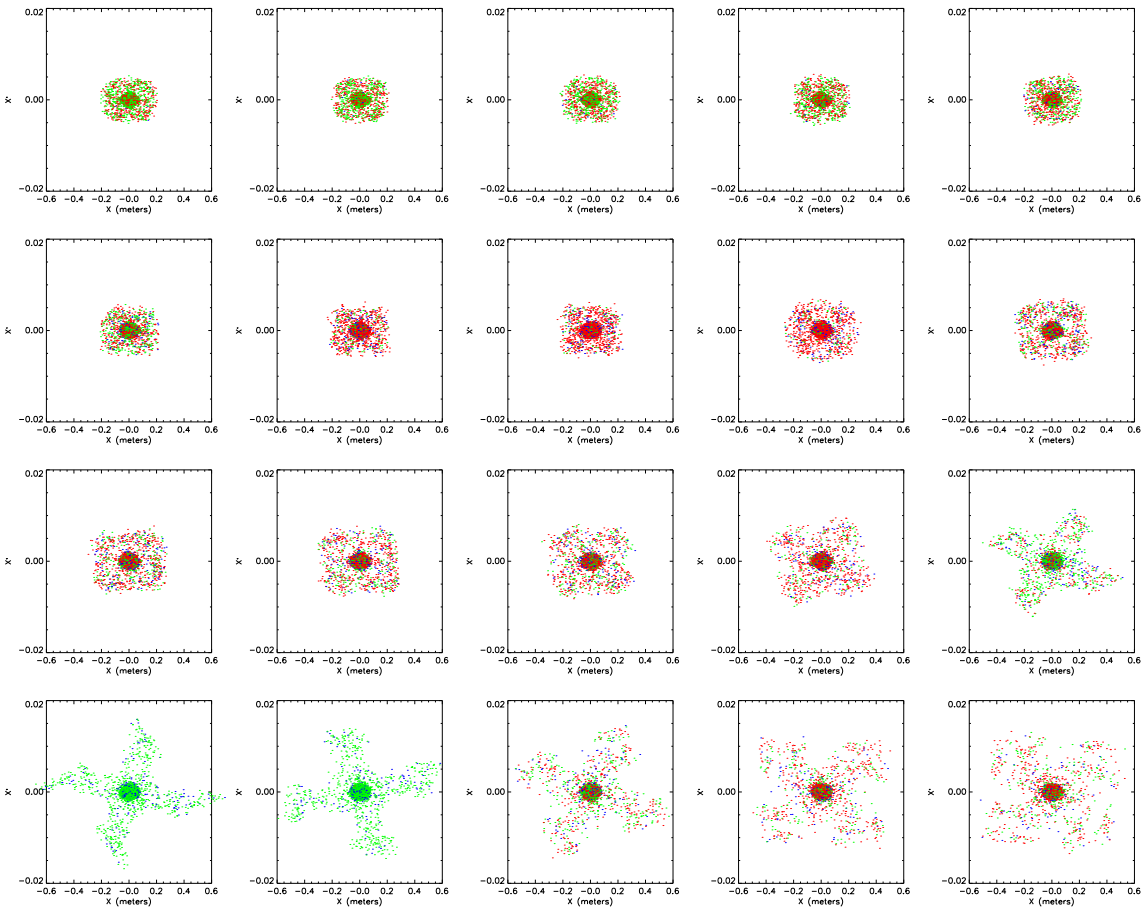

Figure 4.23: SYSTEM 1: Trace-space projections (x v. x') of the beam at various times starting at 310 turns and moving to 500 turns. This area shows the emittance growth of the beam, and has been investigated to watch this increase in detail. This is the 1×10^{13} particles per meter space-charge regime. Red denotes chaotic orbits, green sticky and blue regular.

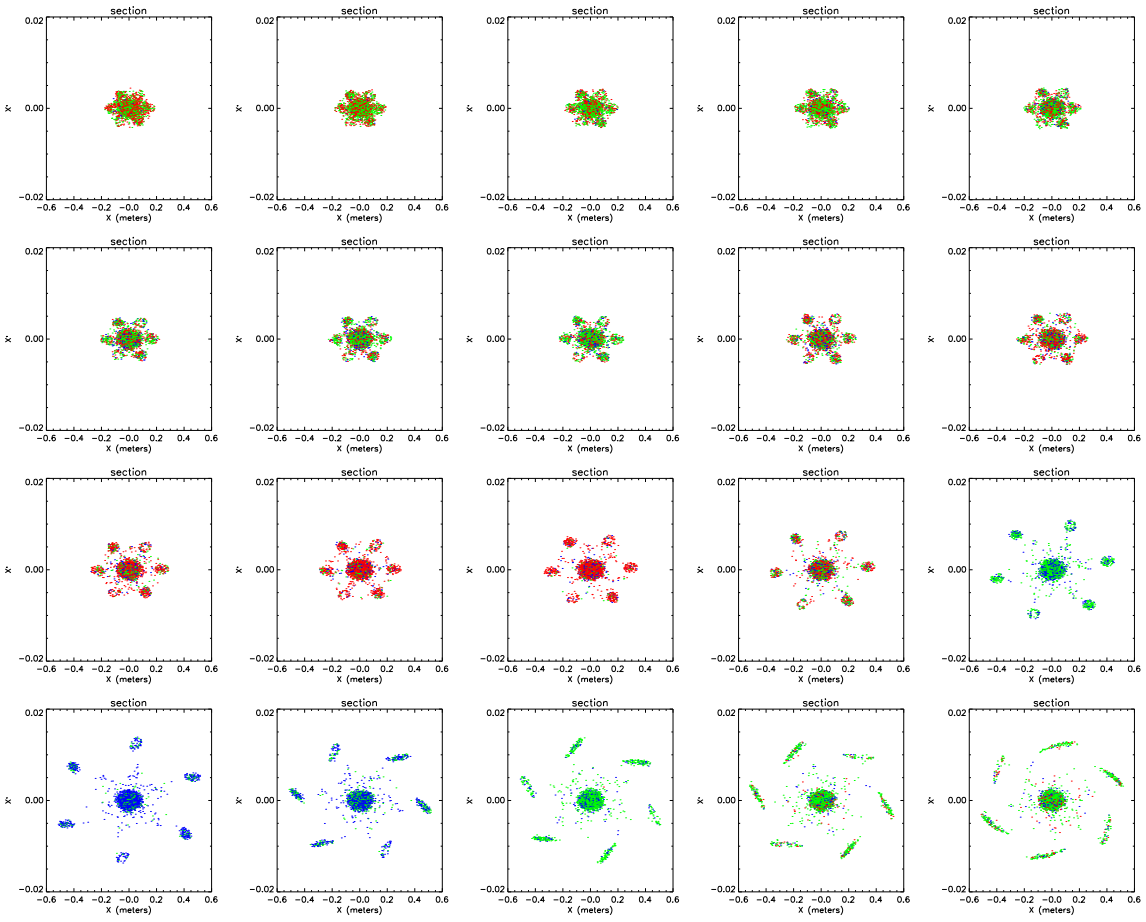

Figure 4.24: SYSTEM 2: These are trace-space projections (x v. x') of the beam at various times starting at 310 turns and moving to 500 turns. This area shows the emittance growth of the beam, and has been investigated to watch this increase in detail. This is the 1×10^{13} particles per meter space-charge regime. Red denotes chaotic orbits, green sticky and blue regular.

4.4 Tune Maps

Since the space-charge of the system affects the way that the beam evolves, the betatron-tune acting on a test particle is not necessarily the tune that is put into the map. Therefore, it is a good idea to calculate it.

4.4.1 Tune Averages

When the tunes for each turn are averaged, we can see that one of the effects of space-charge is that, early in the beam's evolution, it is drawn away from where the ramping wants it. In fact, it would appear that in high space-charge regimes resonance is never reached.

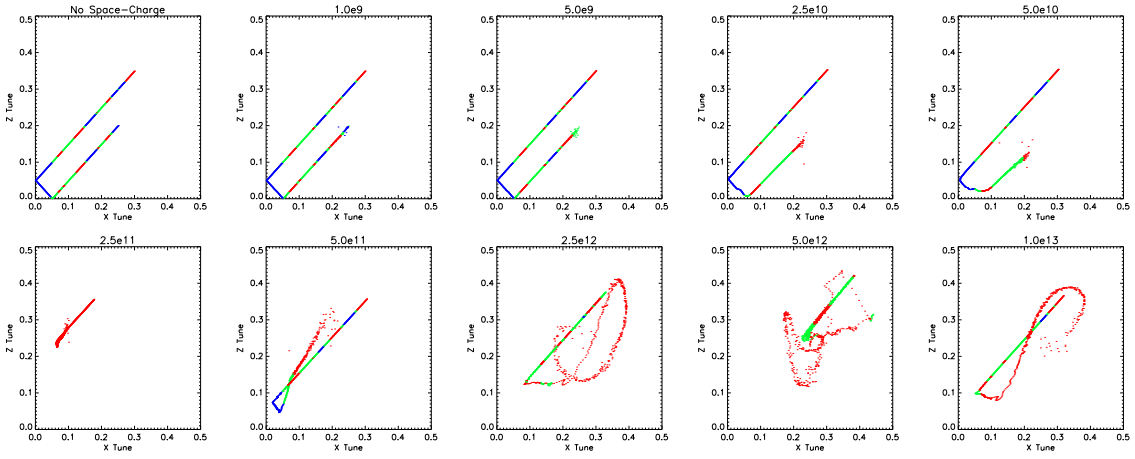

Figure 4.25: The average betatron-tunes for each turn along with their average chaos level, plotted for System 1. Red denotes a turn that was on average chaotic, green sticky, and blue regular. Their space-charge densities are listed above each plot.

However, we must remember that Figures 4.25 and 4.26 merely show the average

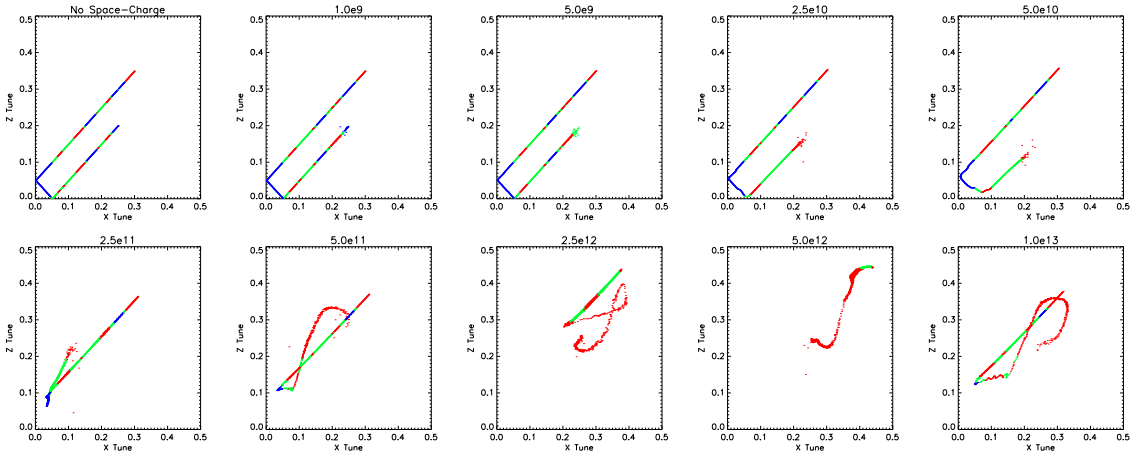

Figure 4.26: The average betatron-tunes for each turn along with their average chaos level, plotted for System 2. Red denotes a turn that was on average chaotic, green sticky, and blue regular. Their space-charge densities are listed above each plot.

of the tunes, and since many of these orbits are chaotic, we would expect them to take on a number of tunes.

4.4.2 Individual Orbits

This work has mostly dealt with plots of statistical properties and snapshots of the beam in time. From it, we have drawn conclusions about the role of regularity and chaos in the evolution of the beam, as well as inferred how the beam evolves in time. Such inferences (i.e. that the resonance creates regular islands that expand outwards) must be tested. Therefore, it would be instructive to examine the manner in which individual orbits evolve through trace-space in relation to their betatron-tune.

Since different initial conditions will lead to different results depending on the

tune of the system and the space-charge regime that was selected, a group of orbits was chosen for their ability to reflect various actions of the beam as it evolves. Since comparing the same initial conditions for different betatron-tune systems would not provide a valid comparison, they will be split up in this particular examination.

4.4.2.1 System 2: $\nu_{x0} = 4.25$, $\nu_{z0} = 4.20$

Figure 4.27 was chosen since it shows a wide range of behaviors germane to this study. In every frame in which the tune comes within proximity of $\nu_x = 0$, while at the same time experiencing a period of regularity, we can see a definite pattern emerge in the signal. This is particularly evident in the $0 \rightarrow 5 \times 10^{10}$ regimes, which we identify as the resonance condition.

In the 5×10^{11} regime, we can see the behavior we expect: the particle starts out in a small hexagonal orbit, then spirals around an expanding island before being trapped in a larger outside orbit. We can see the resonance phenomenon as the tune approaches zero and there is an increase in regularity. In other examples, such as the 2.5×10^{11} and 5×10^{10} regimes, the resonance relaxes the orbit to a smaller state. These are examples of the orbits left behind when the islands expand outwards.

Figure 4.28 was selected because not only is there a small resonance phenomenon in the 2.5×10^{11} regime (which does not grow as explosively as in the previous example), but there is a very striking example of this resonance island growth in the 1×10^{13} regime. Although this type of expansion for a space-charge regime is rare, it does exist, and shows that when the orbits are far from the center they will behave as if they were subjected to a lower space-charge regime.

Figure 4.29 shows a number of different expansions. There are the small expansions at resonance of the 5×10^{10} and 2.5×10^{11} regimes. There is an interesting expansion in the 5×10^{11} regime where the original orbit in the island is not regular until the island has moved halfway outwards. Finally, there is the entirely chaotic expansion of the 2.5×10^{12} regime.

These expansions that do not become regular until far away from the center are interesting and may point to some of the mechanisms involved in the emittance growth observed. If we closely examine the tune graph for the 5×10^{11} regime, we notice that, while the initial tunes are spread over a wide area and clearly chaotic, they begin to settle down into the familiar tune ramp graphs seen in the lower space-charge regimes. If we look at the tune maps for those regimes, we see that, before the regularity surrounding the resonance begins, there is a period of stickiness, followed by a period of chaos, followed by a period of stickiness just before the regularity of the resonance condition. It is most likely that this is an example of the chaos that comes from a time-dependant system exerting itself while the particle is trapped in the island.

The 2.5×10^{12} regime shows us a trajectory where it follows the type of expansion we would expect, yet is chaotic the entire time. If we look closely at the trace-space plot we will see that, while it roughly follows the expanding trajectory, it does deviate somewhat from the type of smooth trajectory we might expect. This is most likely the space-charge adding enough uncertainty to the orbit to make it chaotic. While such a mechanism might also be at work in the 5×10^{11} regime, the fact that the tunes do not settle into a regular progression until after the expansion

in the higher space-charge regime, while in the lower it is achieved with the advent of the expansion, the changing tune is a more likely cause.

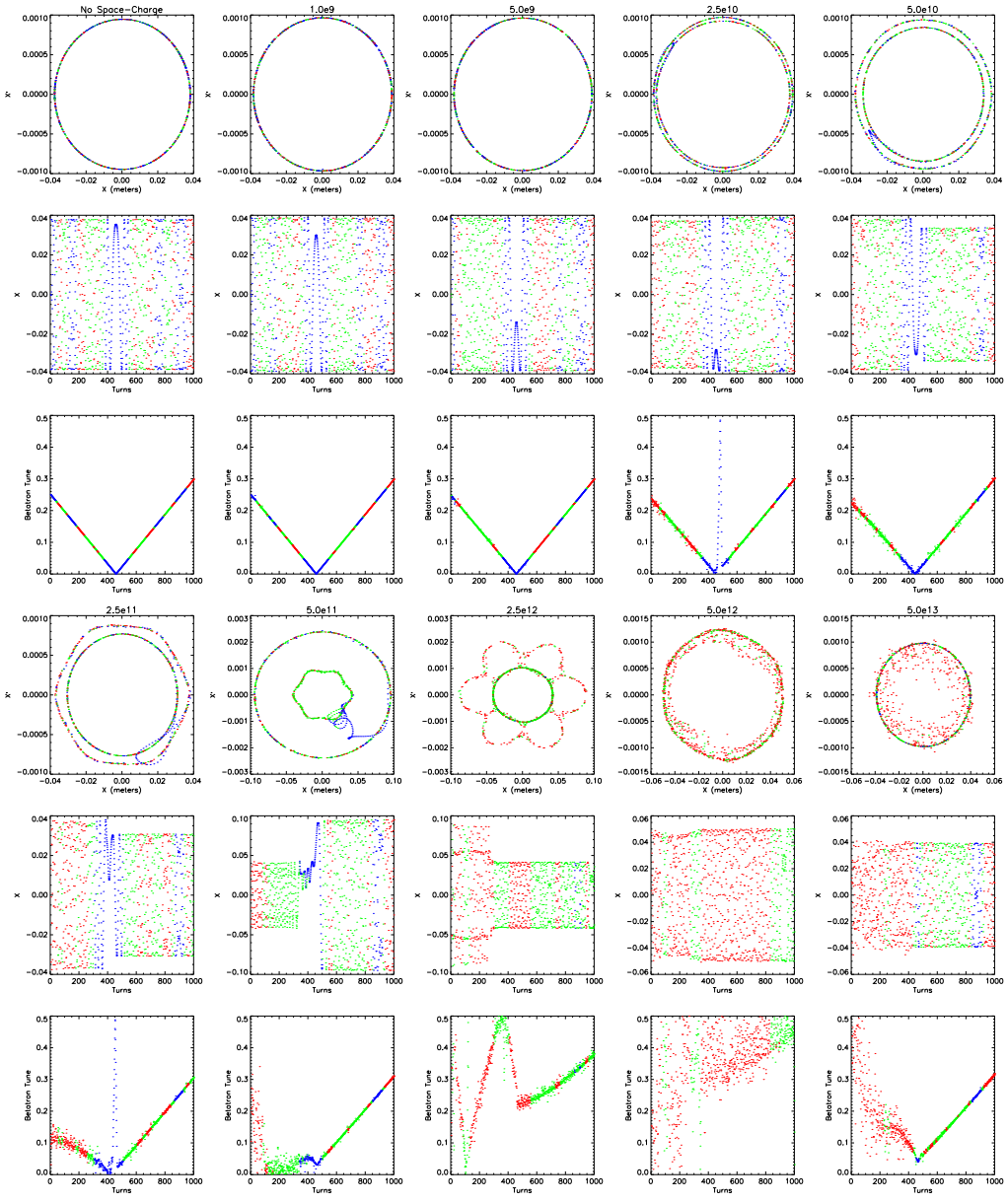

Figure 4.27: Each triplet of rows contains in its first row trace-space plots of the orbit in question, the second row is the x signal with respect to time, the third is the betatron-tune with respect to time. Here red denotes a chaotic point, green sticky, and blue regular. Their space-charge densities are listed above each trace-space plot.

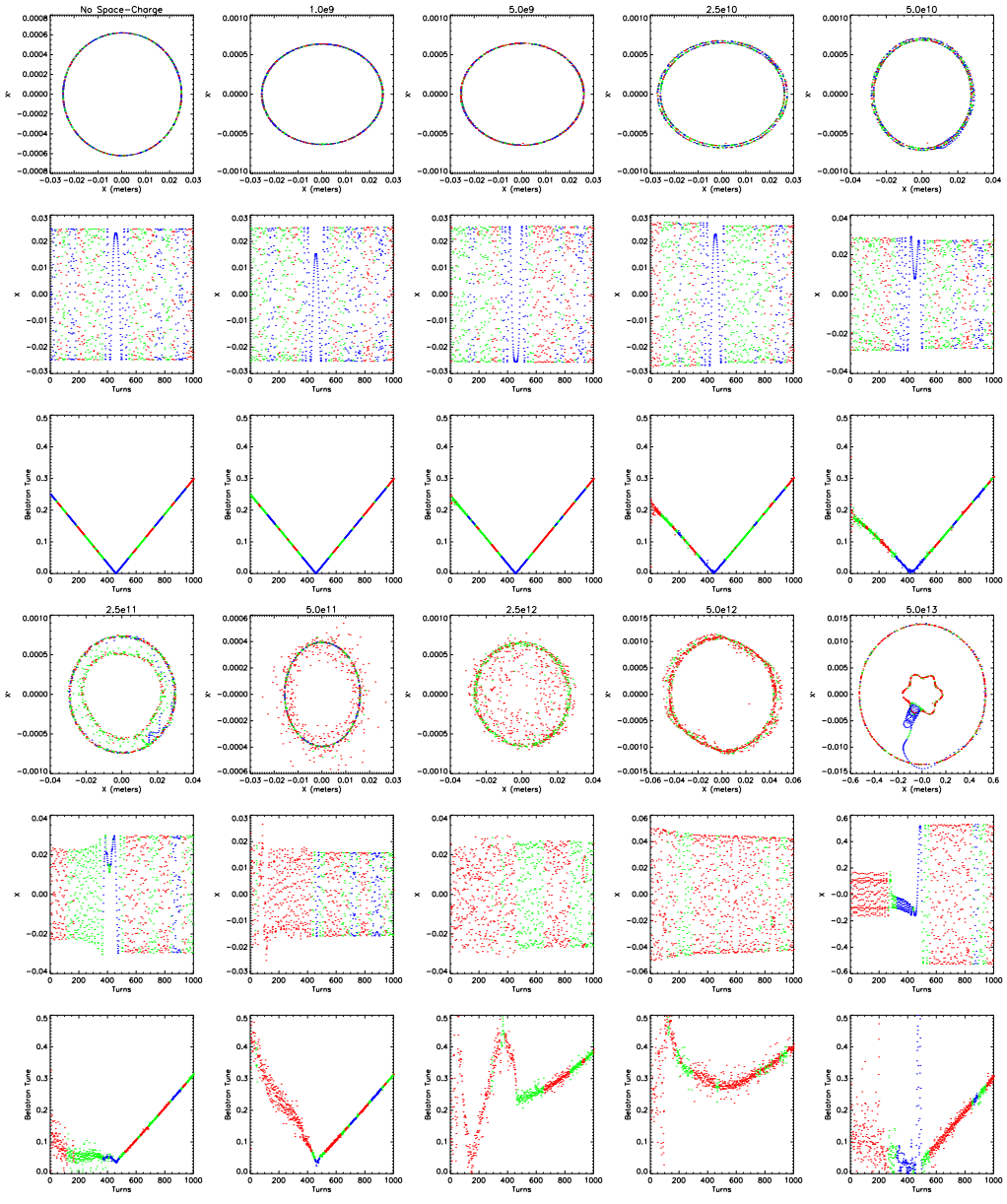

Figure 4.28: Each triplet of rows contains in its first row trace-space plots of the orbit in question, the second row is the x signal with respect to time, the third is the betatron-tune with respect to time. Here red denotes a chaotic point, green sticky, and blue regular. Their space-charge densities are listed above each trace-space plot.

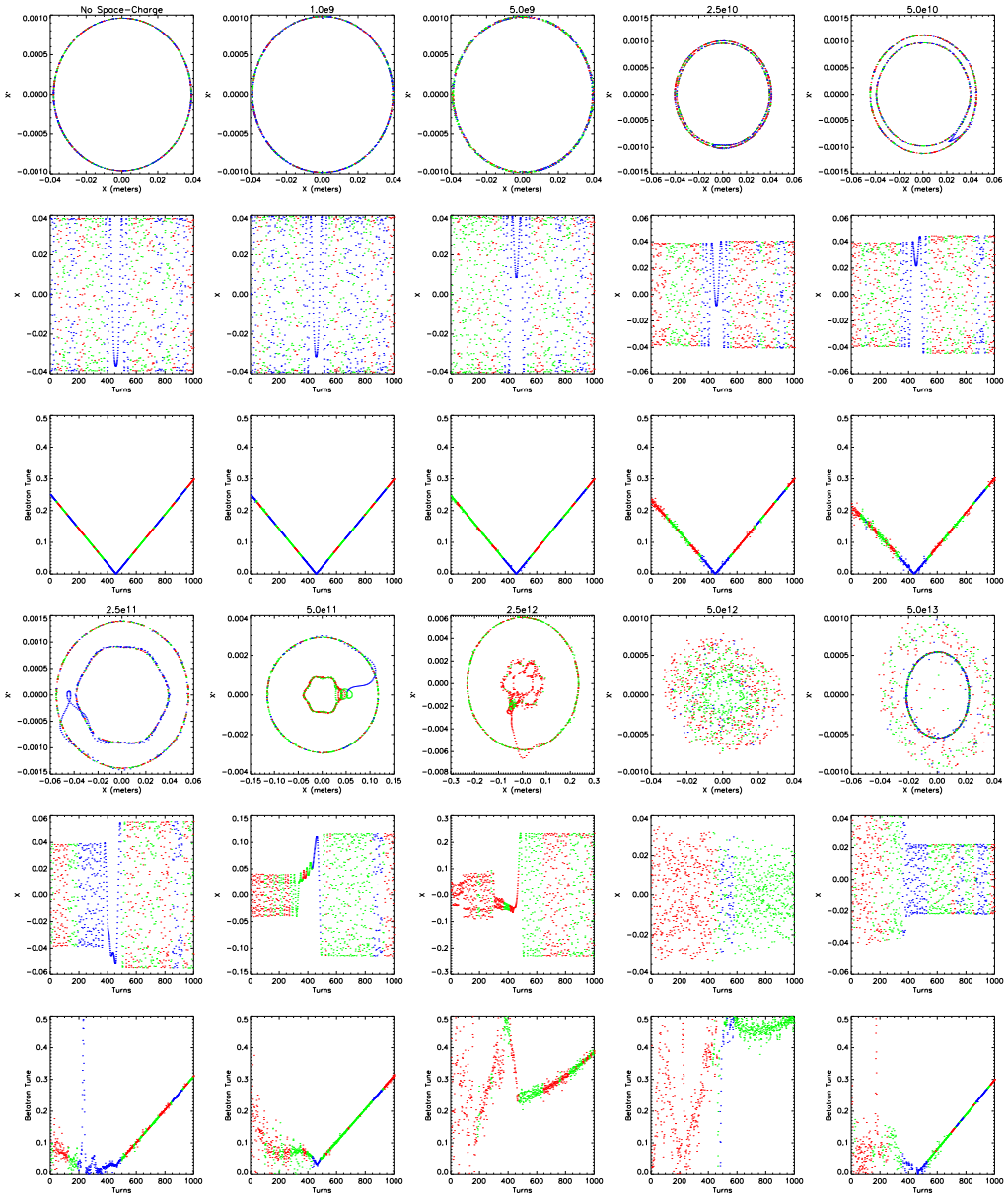

Figure 4.29: Each triplet of rows contains in its first row trace-space plots of the orbit in question, the second row is the x signal with respect to time, the third is the betatron-tune with respect to time. Here red denotes a chaotic point, green sticky, and blue regular. Their space-charge densities are listed above each trace-space plot.

4.4.2.2 System 1: $\nu_{x0} = 6.25$, $\nu_{z0} = 6.20$

Figure 4.30 shows a number of both expansions and contractions related to resonance. The 5×10^{11} regime is interesting in that this particular initial condition begins trapped in an island, and is an excellent example of a resonance-based expansion. Not only that particular orbit, but the 10^{13} regime has its own example of expansion due to resonance. Finally, the 2.5×10^{11} regime has an interesting example of contraction in which it appears to have been caught in an island that brought it into a lower, more stable orbit.

Figure 4.31 shows a number of types of expansion. The 5×10^{10} regime shows an example of the type of small resonance-based expansion we have come to expect, as does the 5×10^{11} regime on a much larger scale. The 2.5×10^{11} regime shows an interesting example of expansion slightly different from what we have come to expect. The particle first rapidly enters an orbit similar to the one in Figure 4.30 where the rectangular nature of the orbit is visible but actual islands have not yet formed. Instead of the rapid expansion that being trapped in an island causes, this orbit remains in a slowly-expanding rectangular orbit until it finally reaches the halo.

Also visible is a 2.5×10^{12} expansion reminiscent of the one in Figure 4.29. It is tempting to label a similar mechanism for such an expansion without a regular resonance condition, but since the expansion occurs so quickly, it is impossible to say that with certainty.

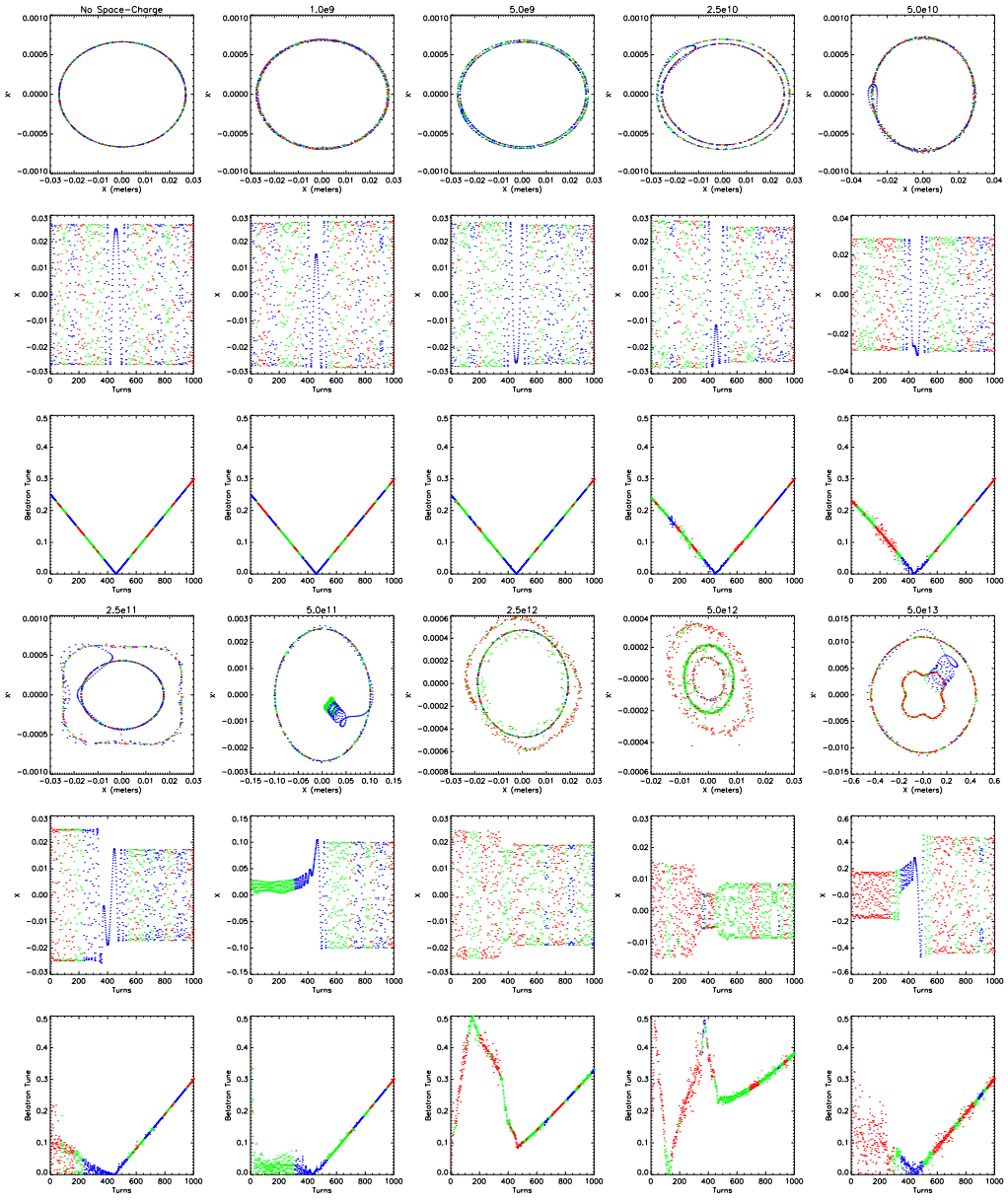

Figure 4.30: Each triplet of rows contains in its first row trace-space plots of the orbit in question, the second row is the x signal with respect to time, the third is the betatron-tune with respect to time. Here red denotes a chaotic point, green sticky, and blue regular. Their space-charge densities are listed above each trace-space plot.

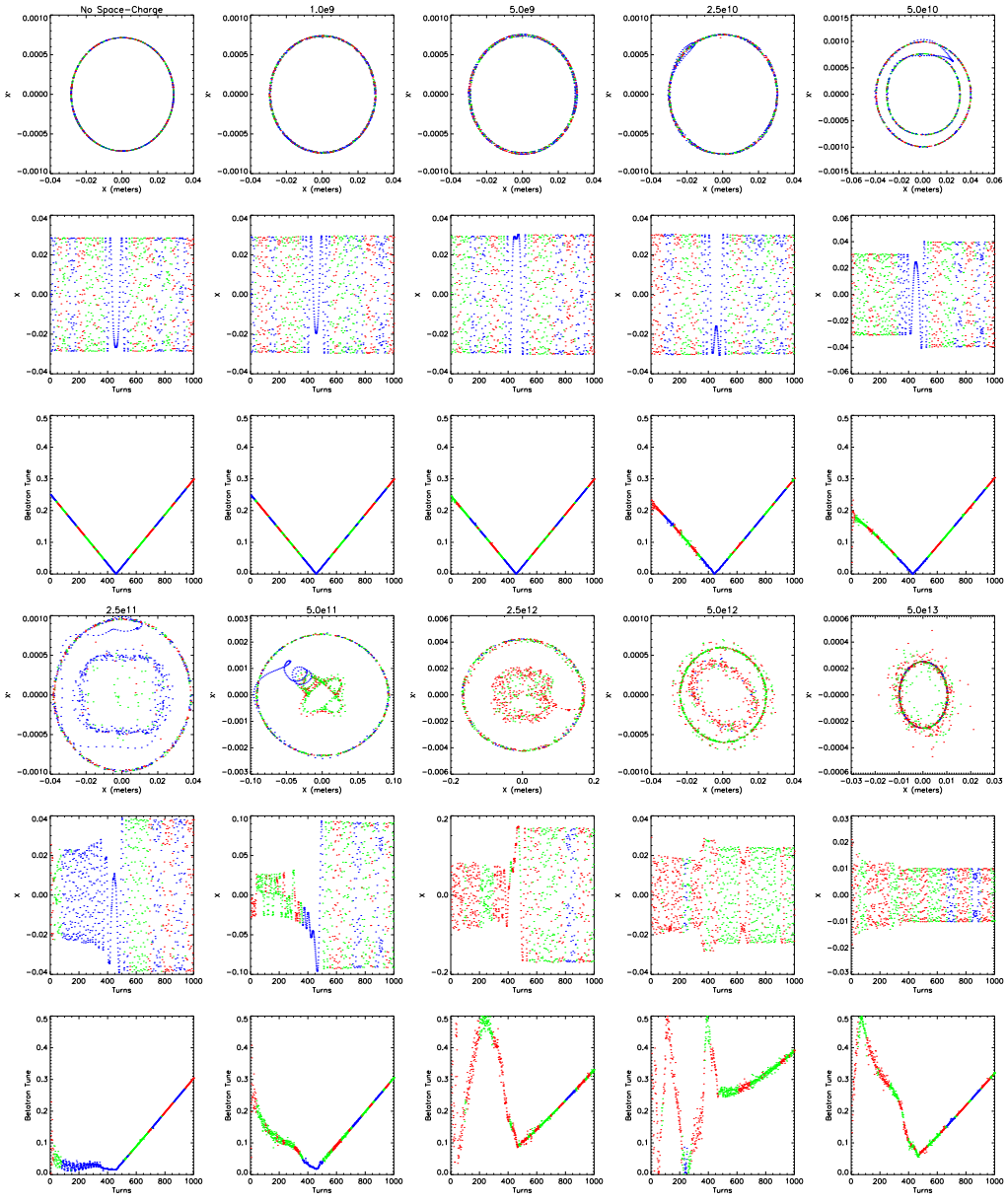

Figure 4.31: Each triplet of rows contains in its first row trace-space plots of the orbit in question, the second row is the x signal with respect to time, the third is the betatron-tune with respect to time. Here red denotes a chaotic point, green sticky, and blue regular. Their space-charge densities are listed above each trace-space plot.

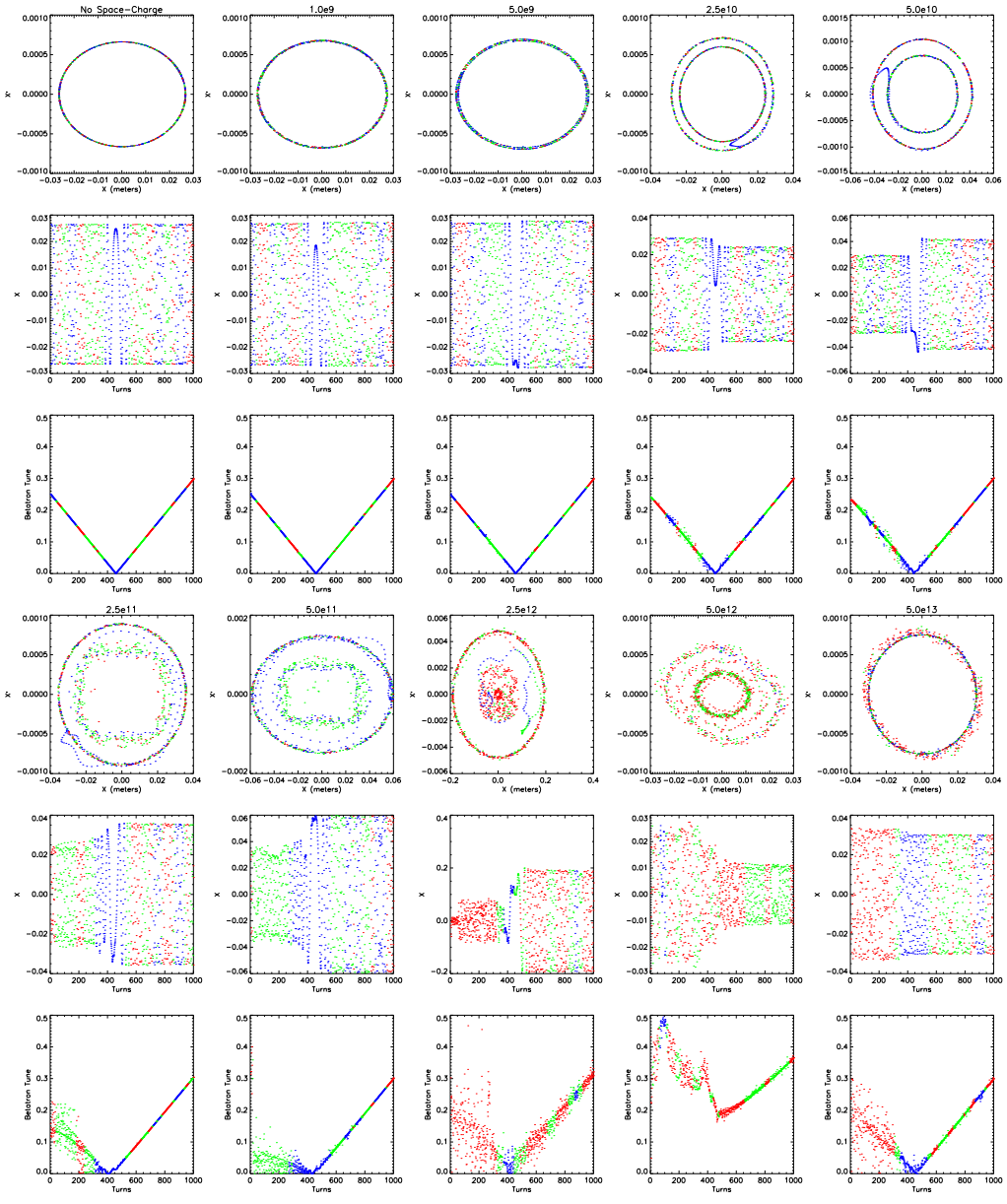

Figure 4.32: Each triplet of rows contains in its first row trace-space plots of the orbit in question, the second row is the x signal with respect to time, the third is the betatron-tune with respect to time. Here red denotes a chaotic point, green sticky, and blue regular. Their space-charge densities are listed above each trace-space plot.

Due to the sheer quantity of orbits generated for this study, it was necessary to restrict what is shown in this work. Examples of most types of orbits can be found in the plots provided. However, occasionally there are some that act in ways different from what we would expect. These are shown in Figure 4.32. While the 10^{11} regimes show small expansions that occur during resonance conditions, there do not appear to be any islands involved. Instead, the particles merely expand slowly as they reach the outer part of their halo.

The other example worth mentioning is the 2.5×10^{12} regime. In most of the orbits we found with drastically increasing emittance, we have seen profound evidence for a particle being trapped in an expanding island before entering a stable outer orbit in the halo. In this case, we see that the particle, far from being trapped, was pulled out by three different islands.

By viewing these individual orbits we can gain a greater understanding of what occurs in the beam. We have seen in the slices of Section 4.3 that in the 10^{11} and 10^{13} space-charge regimes that moving islands pull a number of the particles outwards to form the halo. These orbits show how these actions can occur. We have seen not only the expected phenomena of the orbit traveling in a spiral defined by the island, but also other means of expansion, including orbits that simply spiral outwards, islands that deposit their particles into lower orbits, as well as particles interacting with multiple islands.

These varied mechanisms for emittance growth show that the methods of expansion in a beam are far from homogeneous and, especially in instances where the resonance condition causes a contraction in the trace-space size of the beam,

may point to new methods for controlling emittance increases in future accelerators.

4.4.3 Binned Tune Values and Chaos

Since merely plotting all of the tunemaps at once would be confusing, it was decided to further refine the data. The tune that a particle felt during its preceding turn was calculated, and combined with its irregularity or chaos value. These chaos values were then binned and averaged over ν_x, ν_z space. If no tunes inhabited a particular bin, it was left white. We can see in Figures 4.33 through 4.34 that, as space-charge increases, the number of available tunes increases until it fills the entire spectrum, with regular and sticky areas becoming smaller and smaller. However, they begin to reappear in the highest space-charge regimes. This was, earlier in this work, attributed to particles being thrown far enough out that their space-charge no longer is strong enough to cause this behavior. This study provides the most solid proof yet.

In Figure 4.33, where the low space-charge regimes are shown, we see a great deal of white space. This is because, for the most part, the particles are staying on the line defined by the tune ramping. As the space-charge increases, however, the number of tunes that the beam has available to it increases beginning with regular harmonics and expanding into a wide range occupied by mostly chaotic orbits. These binned tunes are not the whole story, since they only show averages for each tune, they provide no information about how many particles occupy any of these tunes.

So, to fully understand them, we plot the distribution for the life of the beam. This is done by taking the number of times a particle occupies a particular tune-bin

and plotting this distribution as a three-dimensional surface. We see that, while a few of the orbits may briefly enter these other tunes, the vast majority of the beam occupies the tunes determined by the ramping for the vast majority of the time.

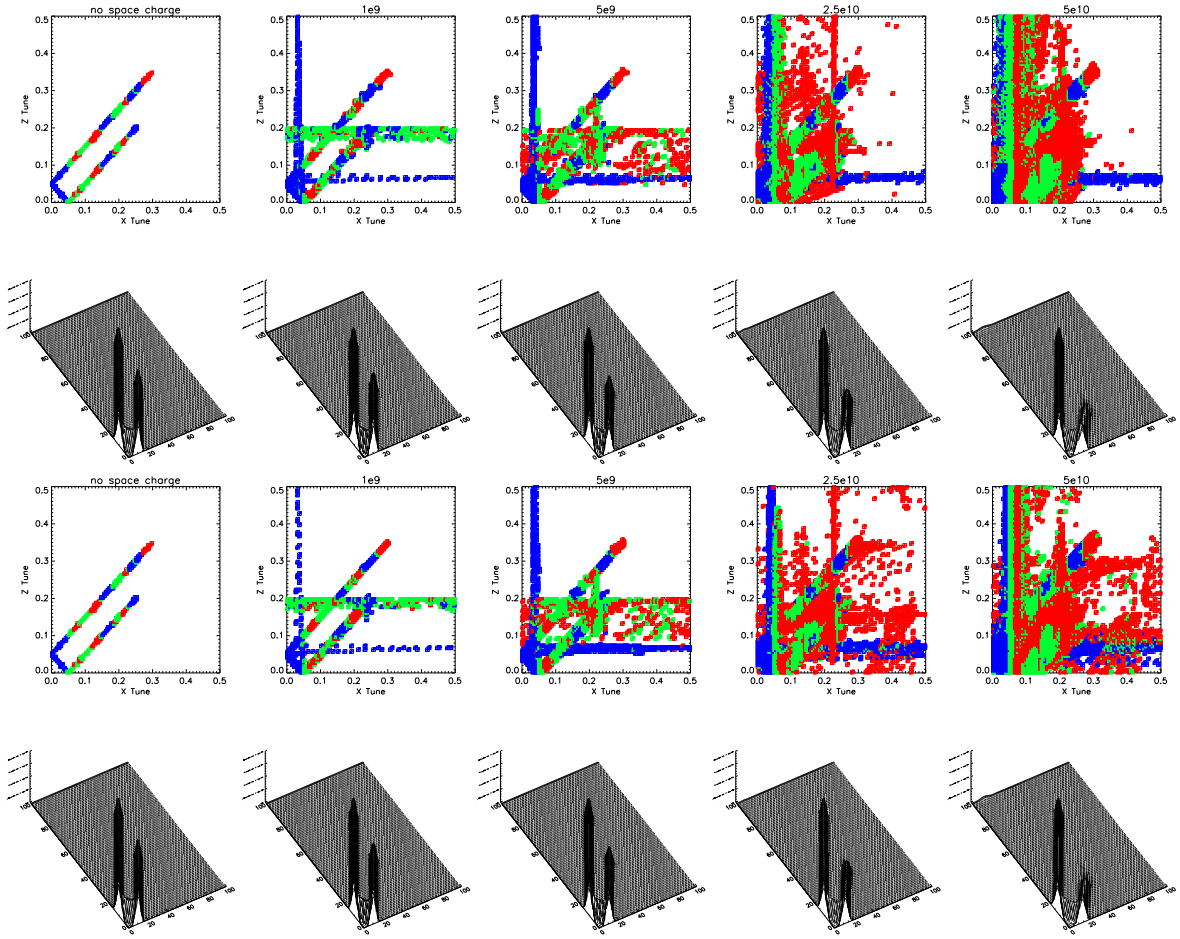

Figure 4.33: The top row of each doublet shows the average amount of chaos distributed across ν_x,ν_z space. Red denotes that that particular tune is on average chaotic, green sticky, blue regular, and white when no orbits reach that tune. The next row denotes the distribution function in tune-space. The top two rows denote System 1 the bottom System 2. These are the low space-charge regimes

When higher space-charges are concerned, as shown in Figure 4.34, there is a great deal more to look at. As is to be expected, the available tunes quickly consume the entire area of tune-space. The plots show that the majority of the area outside the ramp line is on average chaotic. Since one of the definitions of chaos is that it has a very wide spectrum, this is not unexpected. When we look at the distribution graphs we see that these regimes do not follow the line for the ramped tune at the beginning. Instead, they are either spread out or have concentrations either at the upper corner, or in the case of the 2.5×10^{11} regime in System 1 at $\nu_x = 0.05$ and $\nu_z = 0.35$. However, all of these regimes in both systems return to the ramped line commensurate with the end of the ramping cycle. This has been observed in previous parts of this section in the average tune graphs, as well as the tune maps for the individual orbits. Since these regimes involve the formation of a halo, it was postulated that this was caused by the particles being thrown so far out that the space-charge had decreased to the point that it acted like one of the lower space-charge regimes.

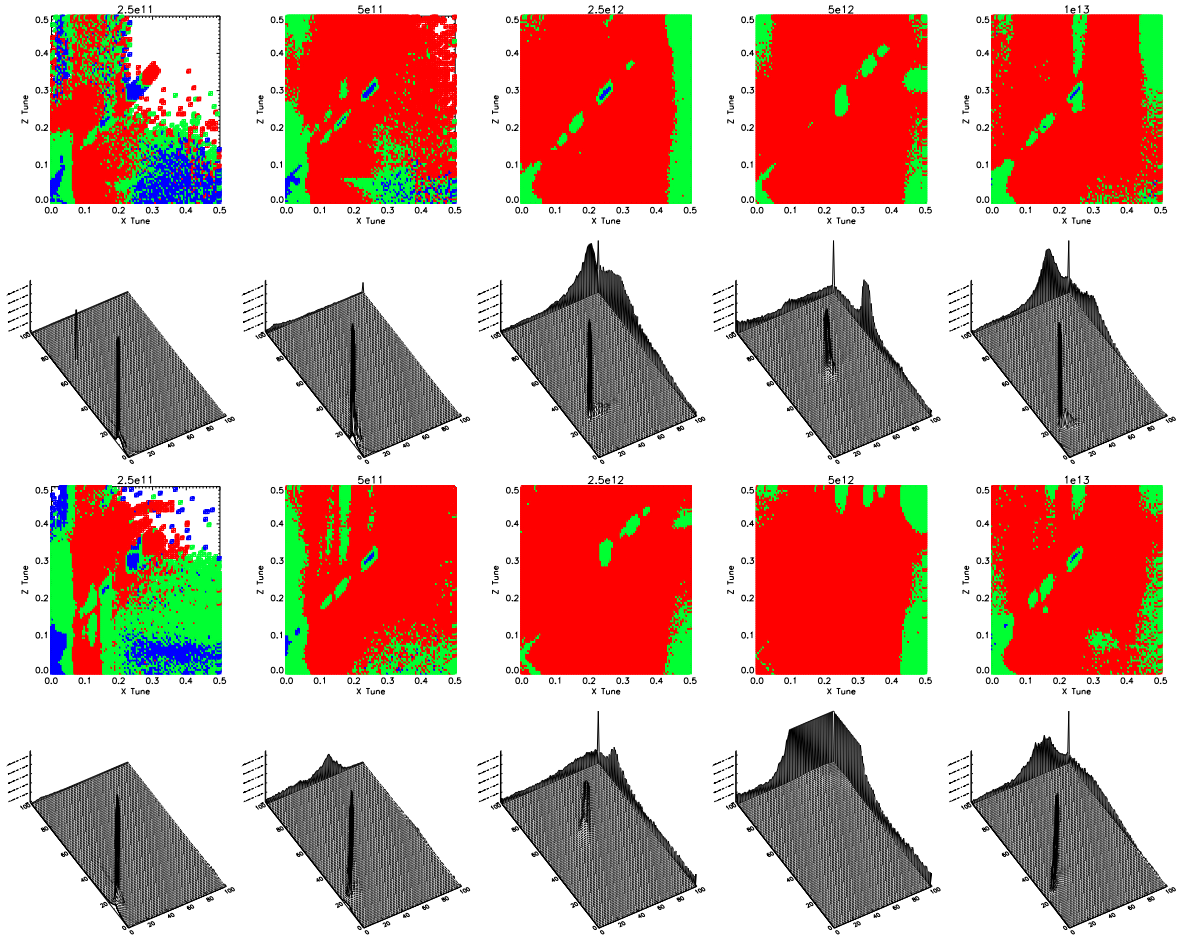

Figure 4.34: The top row of each doublet shows the average amount of chaos distributed across ν_x,ν_z space. Red denotes that that particular tune is on average chaotic, green sticky, blue regular, and white when no orbits reach that tune. The next row denotes the distribution function in tune-space. The top two rows denote System 1 the bottom System 2. These are the high space-charge regimes

In order to show how the binned tunes relate to the space-charge which affects them and the radius at which they reside, these values will be compared. The plots in Figures 4.35 through 4.38 were made by re-plotting the binned tunes with their average chaos. We see the average magnitude of the space-charge force at each tune, and, finally, the average radius of each tune.

The values calculated for the low space-charge regimes in Figures 4.35 and 4.36, are not entirely reliable indicators of what is occuring since they only cover a small area of tune-space. However, in the 10^{10} regimes, we do begin to see some information: the areas of tune-space along the ramping line have a higher average radius than the areas that show the most chaos, as well as a lower amount of space-charge force. Since so little an area of tune-space is shown, it will be difficult to draw conclusions based on these low space-charge examples.

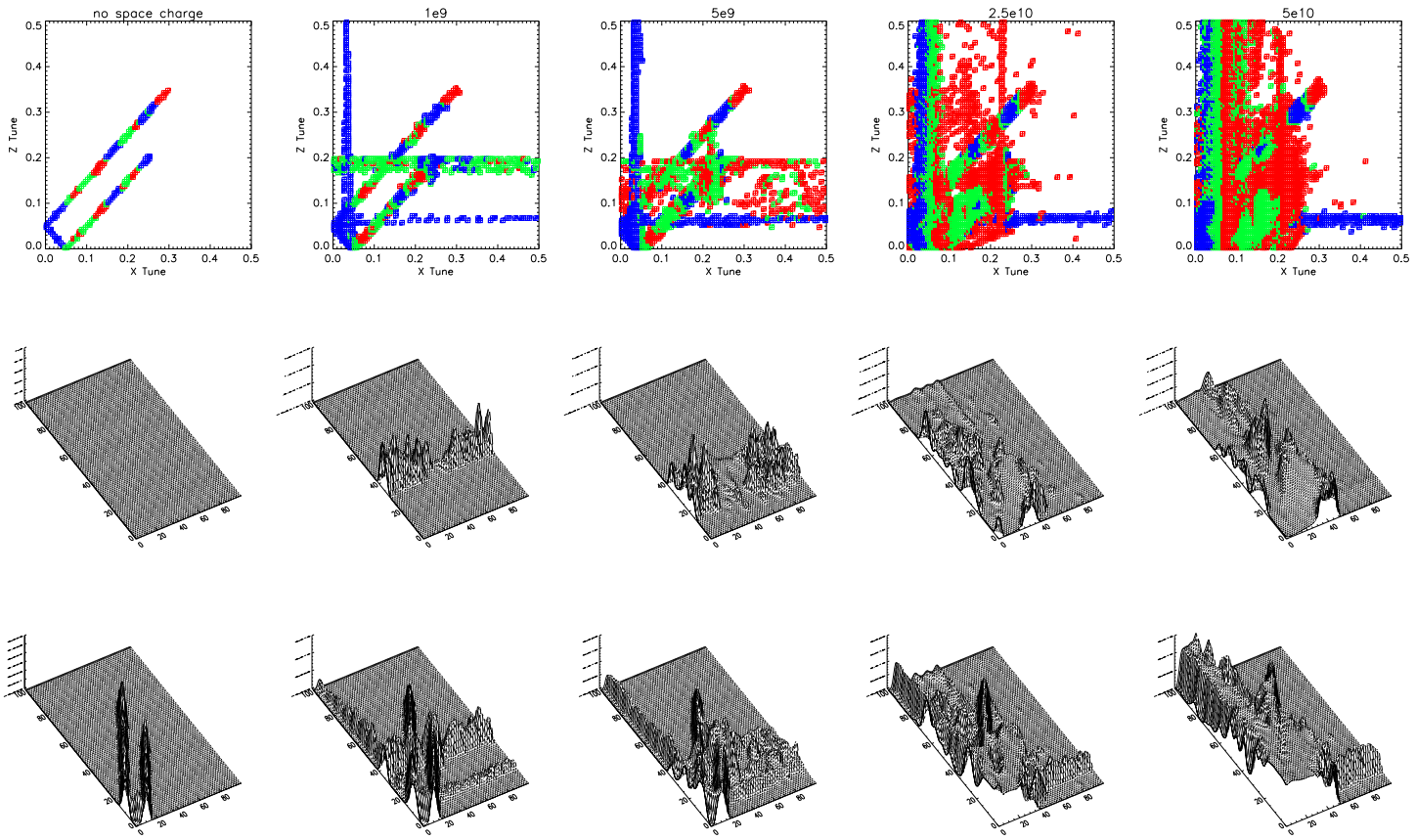

Figure 4.35: The top row shows the average amount of chaos distributed across ν_x,ν_z space. Red denotes that that particular tune is on average chaotic, green sticky, blue regular, and white when no orbits reach that tune. The second row are the average values of the space-charge kick magnitude. Last row denotes the average radius for each tune. These graphs represent System 1.

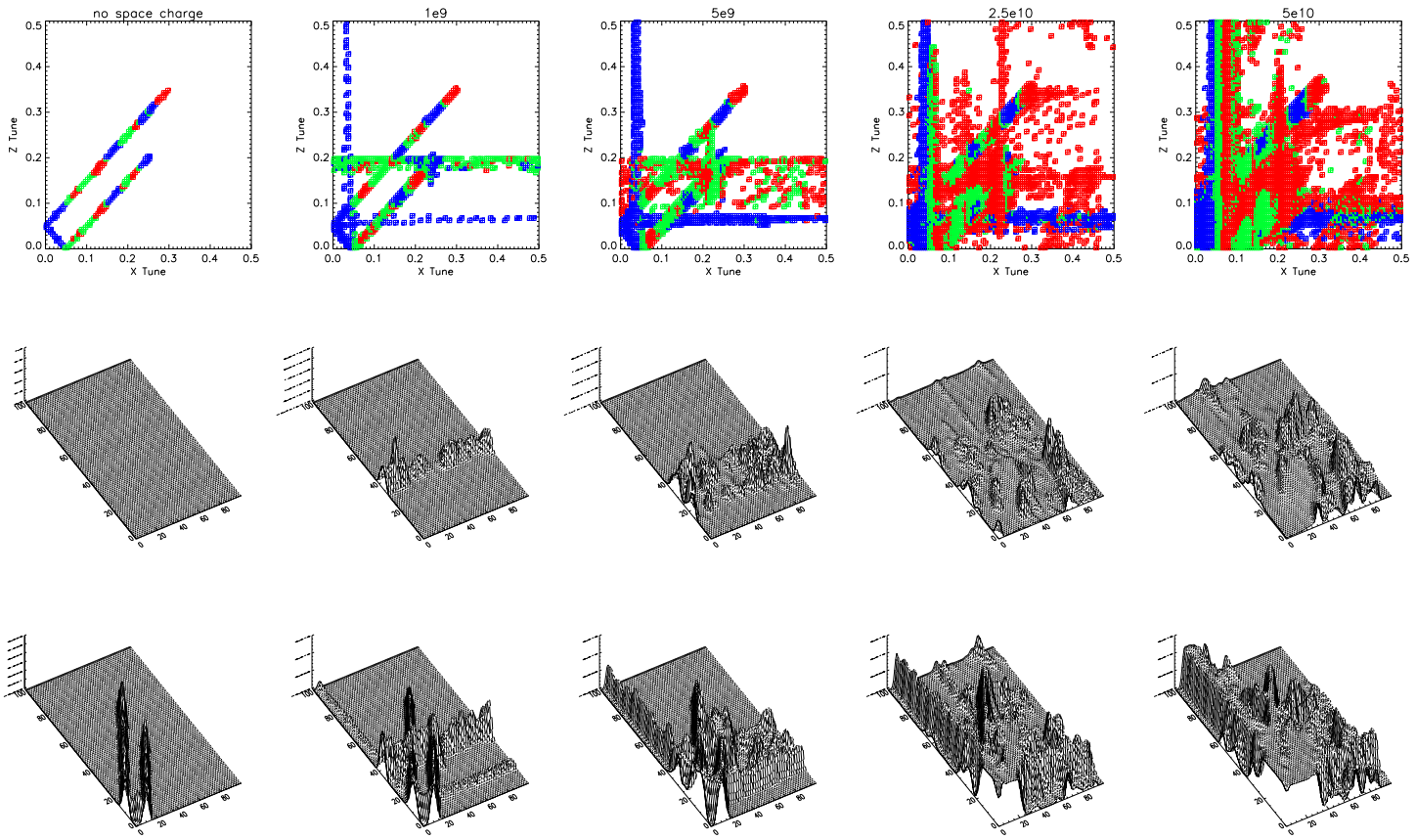

Figure 4.36: The top row shows the average amount of chaos distributed across ν_x,ν_z space. Red denotes that that particular tune is on average chaotic, green sticky, blue regular, and white when no orbits reach that tune. The second row are the average values of the space-charge kick magnitude. Last row denotes the average radius for each tune. These graphs represent System 2.

Finally, when looking at the high space-charge regimes in Figures 4.37 and 4.38 we begin to see what we were looking for. In System 1 we see that along the ramp line corresponding to the post-resonance portion of the beam, the plots describing the space-charge magnitude show a deep trough. This confirms our supposition that this behavior comes from the particles being thrown out into higher orbits since the maximum value for average radius is along the ramp line.

In System 2 we see a slightly different story. In the 10^{11} and 10^{13} regimes we see the same sort of behavior as System 1. When we look at the 2.5×10^{12} regime the similarity is tenuous and in the 5×10^{12} regime is nonexistent. In these cases, the average radius is remarkably uniform throughout tunespace, and the space-charge force shows only tiny hints of the huge troughs seen in other regimes. This indifference to tune appears to be the reason that so few of the particles expanded in this regime during resonance crossings, and why the emittance growth was so much smaller than the rest of the regimes.

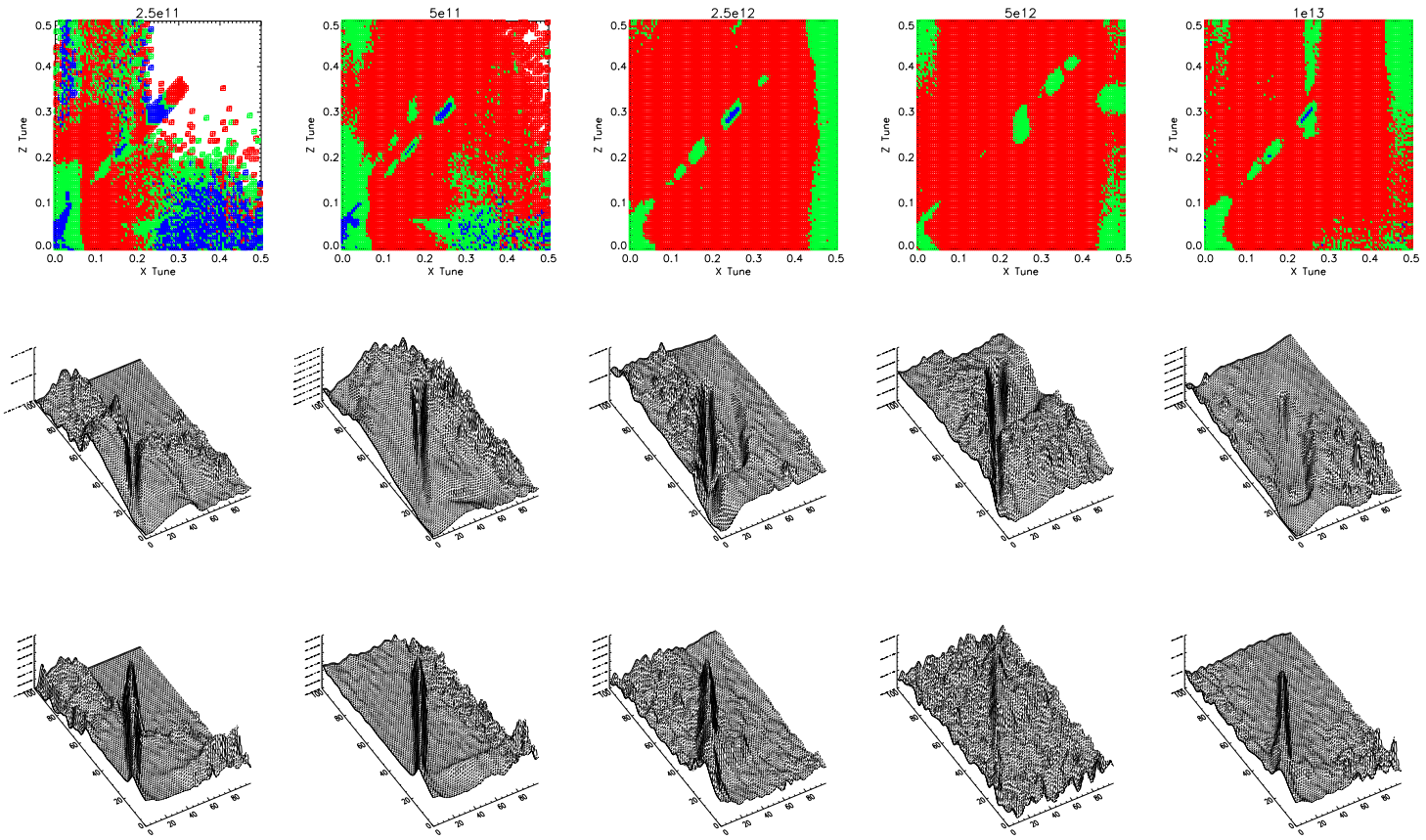

Figure 4.37: The top row shows the average amount of chaos distributed across ν_x,ν_z space. Red denotes that that particular tune is on average chaotic, green sticky, blue regular, and white when no orbits reach that tune. The second row are the average values of the space-charge kick magnitude. Last row denotes the average radius for each tune. These graphs represent System 1.

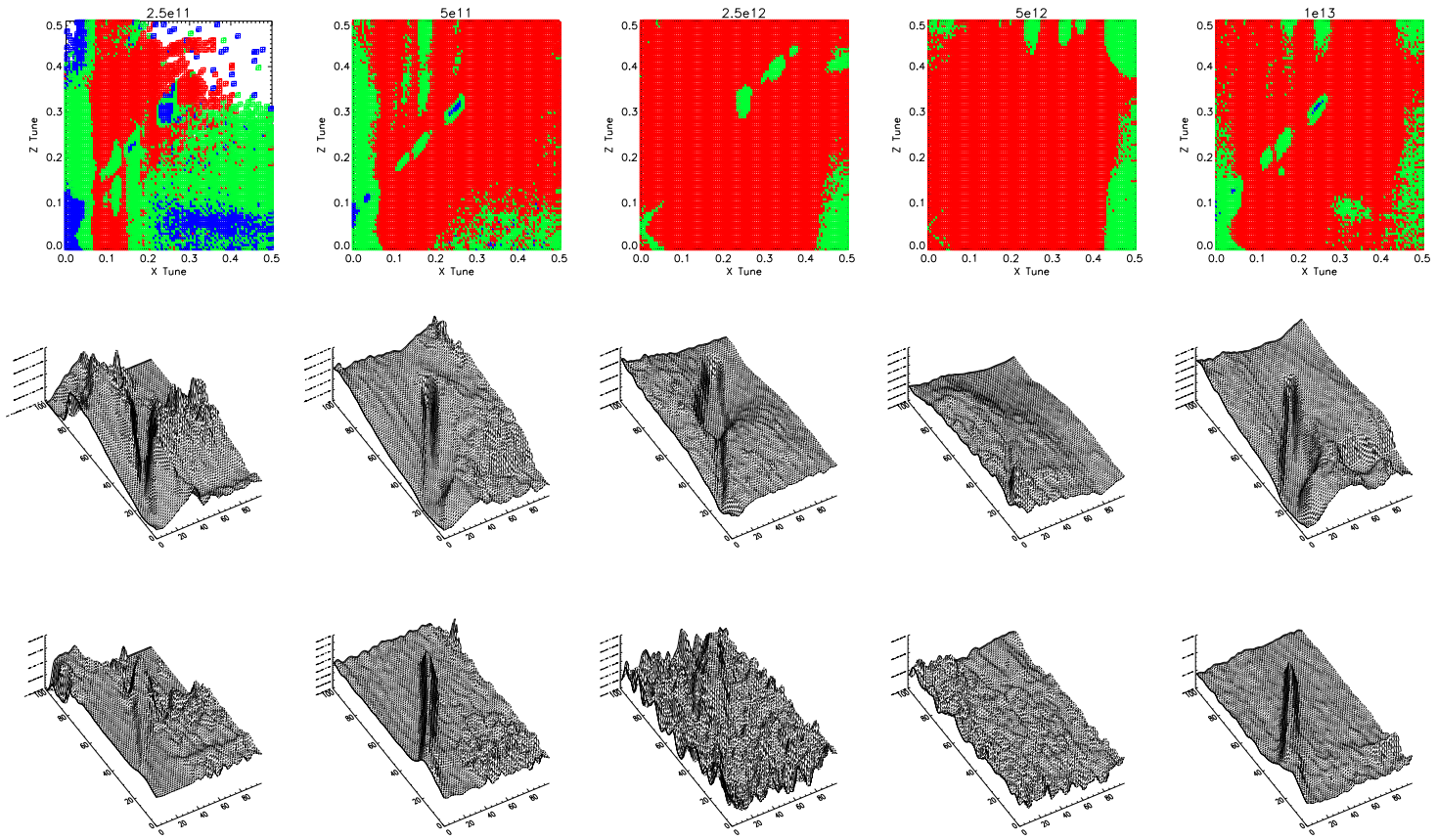

Figure 4.38: The top row shows the average amount of chaos distributed across ν_x,ν_z space. Red denotes that that particular tune is on average chaotic, green sticky, blue regular, and white when no orbits reach that tune. The second row are the average values of the space-charge kick magnitude. Last row denotes the average radius for each tune. These graphs represent System 2.

These plots have helped us see how the beam evolves through tunespace. They have confirmed our supposition that the reason the relative chaos after turn 600 remains relatively unchanged (with exceptions in the 10^{12} regime) is that the space-charge causes the orbits to increase to a high enough radius that the force experienced by the particle is more like force in the lower space-charge regimes.

The 10^{12} regime in general, and the 5×10^{12} regime in particular, seem to be an exception to the observed phenomena. We have seen from the average tune plots that not only does the resonance condition never occur, but that the regime never gets particularly close. Furthermore, the graphs showing the space-charge kick as well as the maximum radius show very little in the way of a pattern. When we compare this to the trace-space slices and emittance growth we see that the emittance growth is small and the vast majority of the particles remain within the central beam. Since the tunes, distributions, space-charge, and radius do not adhere to the behavior seen in other regimes, and also does not experience the large growth in beam size and emittance that the other regimes do, it becomes safe to say that the 5×10^{12} regime is the exception that proves the rule.

CHAPTER 5
CONCLUSIONS

This study analyzed a specific model of a proton beam that assumed a Gaussian potential revised at every turn to reflect the distribution of the particles. 20 different sets of accelerator parameters were used in the experient to determine the effects of different magnitudes of space-charge as well as the effect of two different resonance crossings. The orbits found from this initial calculation were then analyzed to determine the regularity or chaos of each point using the patterns method previously developed by a member of the Northern Illinois Center for Accelerator and Detector Development's Beam Physics and Astrophysics Group.

The study found that for many magnitudes of space-charge the growth mechanism involved the particles becoming trapped in islands which grew as the betatron-tune approached resonance. For some values of space-charge the resonance involved nearly the entire beam becoming regular with a large percentage of the particles entering the halo that was formed. As the space-charge became higher, the effect on the betatron-tunes prevented the majority of the beam's particles from reaching a resonance condition, so only a small number escape into a diffuse halo.

Finally, in the highest examined space-charge regime, the particles are pushed outwards to large radii, which reduces their percieved space-charge, that they begin to feel resonance conditions again. Finally, the study also found that in the model

investigated chaos arises by the simple act of changing the betatron tune even without the interference from space-charge, though an increase in space charge causes more particles to experience chaotic motion.

5.1 Further work

Though the model used in this study had rudimentary implementation of a small level of self-consistency, proper examination of the various systems using a truly self-consistent model would be best. Using a particle-in-cell or other type of self-consistent code to model the system would allow for the verification that the phenomena seen in this model are not model-related, but are in fact based on real physical properties.

Another area for further study is to expand the model into three dimensions. Currently only the transverse dimensions are modeled. While this can be illuminating, the effects of the space charge, especially in the spreading of available tunes, would point to longitudinal effects on the beam shape and distribution.

Within this work, we discovered that emittance growth occurs partially due to moving islands as resonance is crossed. We also discovered that the mechanisms available for expansion are not as homogeneous as we might expect. If a method can be found to classify the various expansion and contraction methods, then determine the relative importance of each in the evolution of a beam, we will gain a greater understanding of how to control emittance growth in future accelerators.

Finally, in the interests of brevity this work dealt almost exclusively with the x dimension. A further study highlighting the z dimension would also be informative.

REFERENCES

[1] Franchetti, G., Hofmann, I., "Modeling of Space Charge Induced Resonance Loss" *AIP Conference Proceedings 642, 2002,* (No. 1): 260-262.

[2] Huang, X., Lee, S.Y., Ng, K.Y., Su, Y., "Emittance Measurement and Modeling for the Fermilab Booster," *Physical Review Special Topics – Accelerators and Beams* **9**, 014202 (2006).

[3] Sideris, I. V., "A Measure of Orbital Stickiness and Chaos Strength," *Physical Review E,* **73**, 066217 (2006).